AD-758 763

ELECTRIC PROBE DATA ANALYSIS FROM TRAIL-BLAZER II-THIRD FLIGHT

Ronald A. Johnson

Avco Systems Division

Prepared for:

Air Force Cambridge Research Laboratories

21 November 1972

DISTRIBUTED BY:

NTIS

National Technical Information Service
U. S. DEPARTMENT OF COMMERCE
5285 Port Royal Road, Springfield Va. 22151

AFCRL-72-0732

AVSD-0461-72-CR

AD 758763

ELECTRIC PROBE DATA ANALYSIS FOR TRAILBLAZER II - THIRD FLIGHT

By

Ronald A. Johnson

Avco Corporation
Systems Division
Wilmington, Massachusetts 01887

Contract No. F19628-72-C-0102
Project No. 4642
Task No. 464202
Unit No. 46420201
Scientific Report No. 2

November 21, 1972

Contract Monitor Dallas T. Hayes
Microwave Physics Laboratory

Approved for public release; distribution unlimited.

Prepared
for

AIR FORCE CAMBRIDGE RESEARCH LABORATORIES
AIR FORCE SYSTEMS COMMAND
UNITED STATES AIR FORCE
BEDFORD, MASSACHUSETTS 01730

60

Qualified requestors may obtain additional copies from the Defense Documentation Center. All others should apply to the National Technical Information Service.

Unclassified

Security Classification

DOCUMENT CONTROL DATA - R & D

(Security classification of title, body of abstract and indexing annotation must be entered when the overall report is classified)

1. ORIGINATING ACTIVITY (Corporate author) Avco Systems Division Wilmington, Massachusetts 01887	2a. REPORT SECURITY CLASSIFICATION Unclassified 2b. GROUP

3. REPORT TITLE

ELECTRIC PROBE DATA ANALYSIS FOR TRAILBLAZER II - THIRD FLIGHT

4. DESCRIPTIVE NOTES (Type of report and inclusive dates)

Scientific Interim

5. AUTHOR(S) (First name, middle initial, last name)

Ronald A. Johnson

6. REPORT DATE November 21, 1972	7a. TOTAL NO. OF PAGES 58	7b. NO. OF REFS 11
8a. CONTRACT OR GRANT NO. F19628-72-C-0102 b. PROJECT NO. 4642-02-01 c. DoD Element 62101F d. DoD Subelement 684642	9a. ORIGINATOR'S REPORT NUMBER(S) AVSD-0136-72CR 9b. OTHER REPORT NO(S) (Any other numbers that may be assigned this report) AFCRL -72-0732	

10. DISTRIBUTION STATEMENT

This document has been approved for public release; its distribution is unlimited. Statement #1

11. SUPPLEMENTARY NOTES Tech, other	12. SPONSORING MILITARY ACTIVITY Air Force Cambridge Research Labs (LZ) L. G. Hanscom Field Bedford, Massachusetts 01730

13. ABSTRACT

The ion current measured by flush mounted electric probes is compared with that predicted from flow field calculations for the Trailblazer II over an altitude range from 220 Kft to 270 Kft. Various approaches, all of which assumed the sheath to be collision-dominated were used to infer ion currents from the flow field predictions. Except for current traces associated with those probes located on the nose cap at 270 Kft, the experimental results were bound from above by the total convective current in the boundary layer and from below by a quasi-one-dimensional current or a diffusion current. The inclusion of convective effects helps provide agreement between theory and experiment for some of the higher altitude data. But over the altitude range considered, it is evident that no simple theory in which it is assumed that either convection, diffusion or a thermal flux respectively is the dominant mechanism for transporting ions into the sheath, produces results consistent with the data. The ion transport phenomena are too complex to be described by such simple theories.

DD FORM 1 NOV 65 1473

Unclassified

Security Classification

Unclassified
Security Classification

14 KEY WORDS	LINK A		LINK B		LINK C	
	ROLE	WT	ROLE	WT	ROLE	WT
Electric Probe						
Plasma Sheath						

Unclassified
Security Classification

AFCRL-72-0732

AVSD-0461-72-CR

ELECTRIC PROBE DATA ANALYSIS FOR TRAILBLAZER II - THIRD FLIGHT

By

Ronald A. Johnson

Avco Corporation
Systems Division
Wilmington, Massachusetts 01887

Contract No. F19628-72-C-0102
Project No. 4642
Task No. 464202
Unit No. 46420201
Scientific Report No. 2

November 21, 1972

Contract Monitor Dallas T. Hayes
Microwave Physics Laboratory

Approved for public release; distribution unlimited.

Prepared
for

AIR FORCE CAMBRIDGE RESEARCH LABORATORIES
AIR FORCE SYSTEMS COMMAND
UNITED STATES AIR FORCE
BEDFORD, MASSACHUSETTS 01730

TABLE OF CONTENTS

I. INTRODUCTION

The determination of the charged particle distribution in the plasma sheath which envelopes a reentry vehicle is important in understanding the electromagnetic response of the vehicle. Hence, the Trailblazer Reentry Test Program was established at AFCRL to allow direct measurements of the electron density distribution in the plasma sheath.

This report is an analysis of ion-collecting electric probe data obtained between altitudes of 220 Kft and 270 Kft for the third flight of Trailblazer II. The blunt-nosed vehicle had a nose radius of .527 ft and a 9° conical afterbody. Its angle of attack during reentry was approximately 10° and it was spinning about its center line axis at approximately 10 revolutions per second. The ion collection data were obtained using three $\frac{1}{4}$-inch diameter flush-mounted copper electrodes that were insulated from the rest of the vehicle surface. The probes were biased at voltages ranging from -5 to -30 volts and were located at the nose cap center point and at S/R = .475 and 2.85 respectively. Here, S is arc distance back from the nose cap center point and R is the nose radius. Positive current traces for these three probes are shown in Figs. 1 through 4.

In analyzing probe data, one can either solve the direct problem, whereby one assumes the flow and chemistry to be known and then predicts the response of the probe to a given applied voltage, or the indirect problem, where one tries to infer the chemistry from the probe current-voltage characteristics. Each method has its advantages and disadvantages. With the direct approach, one may begin with an incorrect ion number density profile and therefore not be able to predict the probe response even if the

mechanism by which ions are transported to the probe is correctly formulated. With the indirect approach, there is the problem of associating a unique chemistry model with the given probe characteristic. In either case, there is the possibility that either the chemistry, the modeling of the ion sheath structure, or both may be incorrect. In this study, the so-called direct approach will be utilized.

To obtain a theoretical prediction of the current as a function of altitude, body position, and applied potential, the charged particle distribution in the boundary layer must be known. To this end, a laminar clean air chemistry model, in which either vibrational equilibrium of vibrational nonequilibrium could be assumed, was used[1,2]. Although it is possible that discrepancies between theory and experiment may be caused by lack of knowledge about the clean air chemistry, the approach taken in this study is to initially assume the clean air chemistry is known.

Theories describing ion collection by electric probes can be very complex depending on the values of such parameters as the ratios of sheath thickness δ_s to ion-neutral mean free path λ_{i-n} or boundary layer thickness $\delta_{b.l.}$. If the former is large, the effects of collisions inside the sheath must be taken into consideration. If the latter is not much less than one, effects of convection within the sheath may have to be considered.

To simplify the data analysis, the experiment was designed with the probe voltages sufficiently large in magnitude that the full random flux of ionized particles of one sign would be collected at the sheath edge. Then a theory[1,3] first proposed by Bredfeldt and Scharfman may be applied to analyze the data. This theory[3] was used by Hayes[1] to infer electron number

densities at a number of altitude and body station combinations for flight number three. Except at an altitude of 270 Kft, there was good agreement between electron number density inferred from the data and that predicted by flow field calculations in the nose cap region of the vehicle. However, the agreement on the conical portion of the vehicle was not good.

Because of this and the dichotomy in the Bredfeld-Scharfman theory of simultaneously assuming a collisionless flux of particles into the outer edge of the sheath and a collision-dominated sheath, it was decided to examine other approaches. As explained in detail in this report, these include a load-line technique that accounts for collisions in the sheath and the large changes in density that may occur across the sheath and an analysis of convection as a possible ion transport mechanism within the sheath. The possibility of current enhancement because of charge depletion near the outer edge of the sheath is also examined.

If the applied potential is sufficiently high that the sheath is many mean-free paths in thickness, the ion drift velocity may be governed by a mobility-limited drift relationship[3]. But, this relationship in only valid if the energy an ion gains in one mean free path is much less than its thermal energy. Keeping this limitation in mind, it was decided to use these other approaches in conjunction with a mobility-limited ion drift to try to achieve better agreement between the data and flow field predictions on the conical portion of the vehicle at all altitudes considered and on the nose cap at 270 Kft.

II. EQUATIONS

If the ion sheath is thin with respect to the boundary layer, convection in the sheath may be neglected and a one-dimensional analysis may be used[4]. However, if the sheath is sufficiently thick that convection can't be neglected within it, two-dimensional effects must be included[5,6]. Since the probe diameter is always considerably smaller than the boundary layer thickness, if convection is important, fringing effects will also be significant. Hence, the problem (cf. Fig. 5) is not only x dependent and y dependent but also z dependent, clearly a most complicated situation.

Even if one assumes that the z dependence can be approximately accounted for by applying a correction factor to a solution that assumes $\frac{\partial}{\partial z} = 0$, the problem is still forbidding. The full equations describing the motion of the electrons and ions over the electrode are, assuming a steady state,

Ion Cont. $$\nabla \cdot N_i \left(U + K_i \nabla V - D_i \frac{\nabla N_i}{N_i}\right) = 0 \qquad (1)$$

Electron Cont. $$\nabla \cdot N_e \left(U - K_e \nabla V - D_e \frac{\nabla N_e}{N_e}\right) = 0 \qquad (2)$$

Poisson $$\nabla^2 V = -\frac{e}{\varepsilon_o}(N_i - N_e) \qquad (3)$$

where V is the potential

N_i is the ion number density

N_e is the electron number density

ε_o is the dielectric constant for a vacuum

U is the velocity of the neutral particles

D_i is the ion diffusion coefficient

D_e is the electron diffusion coefficient

K_i is the ionic mobility

K_e is the electron mobility

It is assumed here that the gas is only slightly ionized so the velocity and temperature profiles for the neutrals can be determined independently of the species conservation equations.

Inside the ion sheath, $N_e = 0$ so

$$N_i = \frac{-\varepsilon_o}{e} \nabla^2 V$$

$$\nabla \cdot \left\{ N_i \left(U + K_i \nabla V - D_i \frac{\nabla N_i}{N_i} \right) \right\} = 0$$

or

$$\nabla \cdot \left\{ \nabla^2 V \left(U + K_i \nabla V - D_i \underline{\frac{\nabla \nabla^2 V}{\nabla^2 V}} \right) \right\} = 0 \qquad (4)$$

Equation (4) is a fourth order partial nonlinear equation in the potential V. Cumbersome numerical techniques[7] have been employed in an attempt to intergrate Eqn. (4). Dukowicz[5] simplified Eqn. (4) somewhat by neglecting the underlined diffusion term. He solved the problem numerically for an incompressible inviscid flow past an ion-collecting flat-plate probe. His

solutions are valid for a constant convective velocity and ion number density upstream of the electrode. Hence, they are not applicable to a reentry boundary layer problem.

In the regime where convective and charge depletion effects are small, but where property variations across the sheath are significant, one can utilize a so-called "load-line" technique[8] to predict the response of the probe to a given applied potential. The load line equation is derived from Eqn. (4) by letting $\frac{\partial}{\partial x} = \frac{\partial}{\partial z} = 0$, and neglecting convection and diffusion. Then the flow of ions is one-dimensional with the ion continuity equation becoming (cf. Fig. 6)

$$j = e\, N_i\, v_i \tag{5}$$

where the velocity of the ions $v_i = K_i E$ is toward the wall as is the ion current density j.

Combining Eqn. (5) with Poissons Equation:

$$N_i = \frac{\varepsilon_o}{e} \frac{d\,E}{dy} \tag{6}$$

results in the differential form of the load line equation

$$j = \varepsilon_o\, K_i\, E \frac{d\,E}{dy} \tag{7}$$

With $j = J_{LL}$ being constant across the sheath. Integrating Eqn. (7) across the sheath and applying the boundary conditions $V(\delta_s) = E(\delta_s) = 0$, $V(0) = V_w$, leads to the load-line equation:

$$V_w = \int_{\delta_s}^{0} \left\{ \frac{2\,j}{\varepsilon_o} \int_{\delta_s}^{y'} \frac{dy''}{K_i(y'')} \right\}^{1/2} dy' \tag{8}$$

where E is the electric field. Since j is constant for a given $\mathcal{F}_s$, Eqn. (8) can be solved for j in terms of a double integral over the sheath. For a given V_w and $\mathcal{F}_s$, it describes the ability of an electric sheath to transport a certain flux of ions by means of a mobility-limited drift. By maintaining the option of allowing K_i to vary, the large variation in properties through the boundary layer are taken into account.

A Fortran listing for the computer code that both computes the load-line current J_{LL} and other relevant quantities may be found in the appendix.

At a given altitude and body-station combination, the following profiles from a boundary layer program are input as functions of distance y out from the wall. They are density ρ(RHO), temperature ratio T/T_e (THETA), ion = electron number density N_i (ED), and velocity ratio u/u_e (FP). Here, T refers to temperature, u to velocity in the x direction, and the subscript "e" refers to conditions at the outer edge of the boundary layer. The particular boundary layer profiles used for this study were obtained by Lew of GE.[2] His profile data are given at thirty unequally spaced points throughout the boundary layer. To obtain values of this data at other y coordinates in the boundary layer, subroutine GETRHØ is used. In this subroutine, a Lagrangian three-point interpolation scheme is used to find values for the dependent variable at the desired mesh points.

The convective current density j_c is found simply from the product

$$j_c = e\, u\, N_i \tag{9}$$

The integrated convective current density is found from

$$J_c = \frac{1}{l_p} \int_0^{y_e} j_c \, dy \tag{10}$$

where d_p is the probe diameter $\approx$ .63 cm. The integration is performed by using Simpson's rule.

The diffusion current density J_d is obtained from

$$J_d = e\, D_i \, \frac{dN_i}{dy} \tag{11}$$

where the derivative $\frac{dN_i}{dy}$ is found by using a central difference formula and the diffusion coefficient D_i is found from the Einstein relation

$$K_i = \frac{eD_i}{kT} \tag{12}$$

and a curve fit for Mason's calculations for the mobility

$$K_i = 4\, \rho_o/\rho \quad \frac{cm^2}{v\text{-}sec} \tag{13}$$

The constant density load-line current J_{LLCD} is found by first of all finding the average density $\bar{\rho} = \delta_s^{-1} \int_0^{\delta_s} \rho(y)\, dy$ throughout the sheath, using Eqn. (v) to calculate the average mobility K_i and then using Eqn. (9) to find J_{LLCD}.

The bulk of the main program is used to find the load-line current density J_{LL}. To do this, Eqns. (4), (6) and (13) are written in the form

$$\frac{d}{dy} E^2 = \frac{\rho j}{4\, \varepsilon_o \rho_o} \tag{14}$$

$$E = -\frac{dV}{dy} \tag{15}$$

For a given sheath thickness $\delta_s < y_{b.l.}$. These equations are integrated in toward the wall using $E(\delta_s) = V(\delta_s) = 0$ as initial conditions. To perform this integration, the subroutine MERKUT is used which is Merson's adaptation of a Runge-Kutta integration scheme. It was found convenient to work in terms of the variables $\tilde{E}^2$ and $\tilde{V}^{2/3}$ where $\tilde{(\ )}$ denotes division by $\sqrt{2J_{LL}}$, in performing this integration. With these variables, J_{LL} did not appear explicitly in the equations. Upon reaching the wall, J_{LL} is found from

$$J_{LL} = \frac{V_w^2}{2\tilde{V}^2(0)}$$

and E and V are found from

$$E = \sqrt{2J_{LL}}\,\tilde{E}$$
$$V = \sqrt{2J_{LL}}\,\tilde{V}$$

The percentage error (as computed by Merson's method) in $\tilde{E}^2$ and $\tilde{V}^{2/3}$ is held to less in one part in 10^5. By picking a number of different values for δ_s extending from 0 to $y_{b.l.}$, a complete load-line curve can be computed.

To determine the importance of including the proper boundary layer density profile in the sheath equations, a second load-line calculation was performed with the density kept constant at its average value throughout the sheath. For this special case of K_i constant, Eqn. (8) reduces to the continuum equivalent of the Child-Langmuir Law

$$J_{LLCD} = \frac{9}{8}\epsilon_o K_i \frac{V_w^2}{\delta_s^3} \qquad (16)$$

where J_{LLCD} has units of current per unit area.

If convective effects are important and diffusion is negligible, the Quasi-One-Dimensional (Q-1-D) approach discussed in Ref. 9 may be used to provide a rough estimate of the current collected by the probe. The basic idea here is that the ions are convected into the sheath (cf. Fig. 6) and then attracted to the wall by the mobility-limited drift phenomenon. The theory is only valid when flow quantities vary much more strongly in the y than in the x-direction. But, we will apply it to the problem at hand anyway as a means of estimating convective effects.

We first use Eqn. (8) to find the load-line current density. The average convective current density per unit probe area J_c is found from

$$J_c = \frac{1}{d_p} \int_0^{\delta_s} e u_i \, N_i \, dy \qquad (17)$$

where d_p is the electrode diameter. Setting J as calculated by Eqns. (8) and (17) equal to one another allows us to calculate a Q-1-D current density $J_{Q\text{-}1\text{-}D}$ and sheath thickness.

III. ANALYSIS OF DATA

The load-line program has been used to calculate the load-line current J_{LL}, constant density load line current J_{LLCD}, diffusive current J_d, convective current density j_c, and integrated convective current J_c at ten different altitude-body station combinations. Results are shown on Figs. 7-19. The label at the top of each figure indicates the altitude and body station combination of interest. In each case the integrated convective current J_c attains its maximum value, of course, at the outer edge of the boundary layer. This asymptotic value is the maximum current the probe is capable of collecting assuming fringing effects are unimportant in calculating the convective current collected. The convective current density j_c attains a peak value within the boundary layer because the ion number density N_i approaches zero near the outer edge of the boundary layer and the convective velocity u approaches zero near the wall.

At all altitudes the diffusion current neglecting charge depletion effects J_d is at least an order of magnitude less than the convective current J_c that is convected through the entire boundary layer. At that place in the boundary layer where N_i reaches its peak value, the diffusion current approaches zero.

The load-line current density J_{LL} or J_{LLCD} increases as the sheath thickness decreases in accordance with Eqns. (8) and (16). Since much of the experimental data was obtained at probes voltages of -5 and -15 volts, theoretical results are shown at an intermediate value of -10 volts. The results can be scaled for other voltages simply by following a V_w^2 scaling

law. Although only showed explicitly on Fig. 10, J_{LLCD} is generally about 30% lower than J_{LL} over the regime studied.

Experimental results for currents collected as functions of altitude are shown on Figs. 1-4 for V_w = -15 volts. Results of V_w = -5 volts are generally around 30% lower. Except for the probe located at the nose cap center point (S/R = 0), all showed roughly a 30% to 50% fluctuation with angle of attack. Since a probe has a surface area of .316 cm^2, the values must be multiplied by 3.16 to be converted into current densities having units of $amps/cm^2$.

Summary plots of both the experimental and theoretically predicted current densities as functions of arc position along the body S are shown in Figs. 7, 8 and 9. The experimental results are obtained from Figs. 1-4 with the assumption that the peak value of J_{exp} in a given (small) altitude range corresponds to the probe positioned on the windward side of the vehicle. Conversely, the minimum value is obtained when the probe is on the leeward side of the vehicle at the maximum angle of attack $\alpha_{max} = 10^o$. Hence, the nose cap center point location corresponds to S = .09 ft, the probe located at S/R = .475 corresponds to S = .12 feet (windward) and .34 feet (leeward); and the probe located at S/R = 2.58 correspond to S = 1.25 feet (windward) and 1.47 feet (leeward).

Except for currents measured by the probes located on the spherical nose (S/R = 0 and .475) at altitudes close to 270 Kft, all the experimental currents were less than the total current being convected through the boundary layer. Here total current is defined as that being convected through

a cross-section perpendicular to the probe having a width equal to the probe diameter and a height equal to the boundary layer thickness. Since the boundary layer is always many probe diameters in thickness, and the probe is only as wide as one probe diameter at one point, this should definitely be an upper bound on total current being collected by the probe. Even if the ion sheath were to extend to the edge of the boundary layer, not all the ions entering the sheath would be collected because of the way the electric field and convective velocities determine the ion trajectories.

By comparing J_c with J_{exp}, one can conclude that the predicted ion density profiles are plausible except between S/R = 0 and S/R = .475 at z = 270 Kft.

The diffusion current density J_d is always less than J_{exp}. A strictly one-dimensional analysis if the sheath is in a collision-dominated regime would involve use of the relation $J_{LL} = J_d$ to compute the sheath thickness and hence the current density. This results in relatively thin sheaths and current densities at least an order of magnitude less than those measured. The corresponding curves are labeled J_{LL}-d and shown on Figs. 7, 8 and 9. At 270 Kft, J_{LL} is always greater than J_d. In other words, the diffusion process never supplies enough current to satisfy the load-line equation if charge depletion effects are neglected. Hence, at 270 Kft the diffusion current J_d is plotted vs. body station S in Fig. 8. At each S, the plateau value of J_d is chosen.

One possibly significant effect that has not been investigated in detail is the phenomenon of local charge depletion in the boundary layer. As ions are collected by the probe the ion number density immediately outside

the sheath region (and, of course, the electron number density) will be reduced somewhat as ions are removed from the boundary layer. This local reduction in N_i will tend to increase J_d over that which is predicted by the boundary layer program.

If charge depletion is important, then the convective and diffusive terms in Eqn. (1) are certainly important in describing flow phenomenon in the charge depletion region. Inside the sheath, the diffusion term may be important near the outer edge and should not be neglected in the load-line equation. For sheaths sufficiently thick with respect to the boundary layer, the convective term will be important also inside the sheath.

To estimate the order of this effect, the width $2w_d$ of this diffusion region may be estimated from

$$2w_d = 2\sqrt{D_i\ t_{tr}} \qquad (18)$$

where D_i is the ion diffusion coefficient at the outer edge of the sheath and t_{tr} is the flow transit time over the probe. The rate at which ions are convected into this region is

$$2\ e\ N_i\ u\ w_d\ d_p \qquad (19)$$

where d_p = .635 cm is the probe diameter.

If this current is continually being attracted to the probe, the net increase in probe current density will be approximately

$$e\ N_i\ u\ \frac{2w_d}{d_p} \tag{20}$$

For body stations on the nose and on the cone at 220 Kft and 270 Kft, this quantity was evaluated and found to be about 3 J_d on the nose and 10 J_d on the cone. The width of the diffusion region was found to be of the order of d_p. At 220 Kft there is the possibility of the necessary ion current being supplied by charge depletion effects. At 270 Kft the total current in the nose region is still too low to match the data but the current due to convection and charge depletion may be sufficient on the cone.

More detailed calculations need to be performed to clarify this point. The results of preliminary calculations discussed here are shown as solid circles on Figs. 7 and 8.

Although fringing effects undoubtedly would not increase the upper bound previously calculated for J_c, the effective surface area of the probe can be assumed to be enlarged by one quarter of a torus having a centroid at the center of the electrode. The correction factor by

which the actual surface area of the electrode must be multiplied to give an effective collection area for diffusion current is then

$$c = 1 + \pi \frac{\delta_s}{r_p} + 2 \left(\frac{\delta_s}{r_p}\right)^2 \tag{21}$$

This equation is useful only if one can calculate a sheath thickness δ_s. As described earlier, in a region where convective effects dominate over diffusive effects in transporting ions into the sheath, the Q-1-D approach may be used to obtain an estimate of the sheath thickness. Results for current density obtained by this method shows disagreement with the theory by an order of magnitude on the nose. Back on the cone, there is reasonable agreement between theory and experiment at 270 Kft while the Q-1-D current is too low by a factor of 3 to 7 at 220 Kft. The Q-1-D results plotted here are for $V_w = -10$ volts. If we had used, instead, results for $V_w = -15$ volts, the predicted currents would have been twice as high and hence closer to the experiment current. The theoretically predicted voltage variation does not agree with the experimentally measured current increase of roughly a factor of 30% as V_w went from -5 to -15 volts. Hence,

it would be misleading to claim agreement between theory and experiment if we could match the data at one (higher) voltage. This is why a representative voltage of 10 volts was picked for this analysis.

Since the Q-1-D method obviously is not always applicable, and the diffusion current without charge depletion is too small to match the experimental current, a sheath thickness was estimated by setting $J_c = J_{exp}$. The results for a few body-station altitude combinations are shown in Fig. 21. They indicate values of c in Eqn. (21) from about 3 to 30 with the larger values being associated with the higher altitudes. If convection is a significant transport mechanism, these results indicate that fringing effects can be quite important in influencing the total diffusion current collected. Of course, in a regime where fringing effects dominate, the utility of Eqn. (21) becomes very limited.

It should be noted that with all of the continuum theories discussed here, the sheath is many ion-neutral mean free paths in thickness. With sheaths of these thicknesses, it would not be proper to use the thermal drift idea of Ref. 3 to calculate the ion current flowing into the outer edge of the sheath. However, in Ref. 1, the calculated sheath thicknesses were only a few mean free paths or less in thickness. Hence, it might have been consistent in that case to use a thermal drift velocity to calculate an ion flux into the sheath.

The main inconsistancy in using the thermal flux plus the mobility-limited drift relationship simultaneously is that they have different regions of the validity. The former is appropriate when the sheath is

collisionless and the latter when the sheath is collision dominated. It would be of interest to use the thermal flux relation, plus a free fall relationship to derive a load-line type equation. The equation for the ion velocity replacing $v_i = K_i E$ becomes

$$v_i = -(-2eV/m_i + v_s^2)^{\frac{1}{2}} \qquad (22)$$

where v_s is the thermal speed at the outer edge of the sheath and m_i is the mass of an ion. Combining Equations (5) and (22) produces a free molecular load-line equation.[6]

$$\frac{j}{j_{th}} = \frac{\left[2\, \mathcal{V}_o h_i\, W^{\frac{1}{2}} \left(1 + \frac{1}{3} W\right)\right]^2}{\delta_s^2} \qquad (23)$$

where $\mathcal{V}_o^2 = \frac{1}{2}\frac{m_i v_s^2}{k\,T_s}$, $W = \left(1 + \frac{\omega}{v_o^2}\right)^{\frac{1}{2}} - 1$, $\omega = \frac{-eV_W}{kT_s}$, $j_{th} = e\,N_s v_s$ is the thermal current density, N is the ion number density, $h_i = \sqrt{\frac{\varepsilon_o k\,T_s}{N_s\, e^2}}$ is the ion debye length, the subscript s refers to conditions at the outer edge of the sheath, k is the Boltzman factor, and V_w is the applied potential. In deriving Eqn. (23) the same boundary conditions on E and V as before have been applied.

When the only source of current for the sheath is the thermal flux, $j = j_{th}$, and Eqn. (23) can be used to estimate the sheath thickness. Plots of j_{th} vs. y and j_d vs. y are shown on Fig. 22 at z = 270 Kft. Since j_{th} is at most a factor of 3 greater than j_d, neither mechanism is sufficient to supply the experimentally measured current. But, at lower altitudes, j_{th} is an order of magnitude greater than j_d, and hence in rough agreement with the experimentally measured current. This is consistent with the findings of Hayes.[1]

Higher altitude results shown on Fig. 22 indicate the thermal current to be no more than a factor of two larger than the diffusion current in regions where the diffusive flux is toward the probe. Here the thermal flux is calculated using the simple kinetic theory expression for the thermal velocity

$$v_{th} = \sqrt{\frac{8\, k\, T}{\pi\, m_i}} \tag{24}$$

where T is the ion temperature = neutral temperature

m_i is the ion mass

and the thermal flux is

$$j_{th} = \frac{1}{4}\, e\, N_i\, v_{th}$$

This gives essentially the same results as the Bohm drift speed

$$v_B = \sqrt{\frac{3\, k\, T_e}{m_i}} \tag{25}$$

when $T_e = T$. Hence, if the electrons are in thermal equilibrium with the ions, one cannot get a sufficient current to match the data from a thermal flux without large fringing effects.

The fact that the calculations of Ref. 1 indicate the probe inferred number density is higher than the predicted N_i at higher altitudes is consistent with the possibility that convection is important at high altitudes. To see this mathematically, if j_{exp} is the experimental current density and N_i is taken as constant across the sheath;

$$N_i = \frac{4\, j_{exp}}{e\, v_{th}} \tag{26}$$

is the expression for N_i assuming no convection but just a thermal flux. If, in addition to this, a convective flux is assumed to transport ions into the sheath,

$$j_{conv} = e\, u\, N_i \frac{\delta_s}{d_p} \tag{27}$$

is the convective current density.

With both a thermal drift and a convective flux transporting ions into the sheath, the inferred number density will be

$$N_i = \frac{j_{exp}}{\frac{1}{4} e\, v_{th} + eu \frac{\delta_s}{d_p}} \tag{28}$$

which is less than that predicted by Eqn. (26).

It should be noted that if convection is important, one can never discover this by using a strictly one-dimensional method. Instead the one-dimensional approaches will require the sheath to become thinner the higher the current density thus rendering convection to be less important. If convection is important and the sheath thickness is of the order of the probe dimension or greater, then the problem is strongly two-dimensional. Simple analyses such as those discussed in this report can only account for the two-dimensional effects very crudely. To analyze the problem more accurately would require numerical solutions of the relevant equations such as those developed by Boyer et al.[7] These massive computer codes are very cumbersome to work with and are costly because of the large amount of computer time involved.

The expression used for the ionic mobility in the load-line equation was a curve fit of either Mason's[10] or Dukowicz[11] predictions for ionic mobility. Mason assumed the mobility to be dominated by elastic collisions and resonant charge exchange collisions between ions and neutrals. The short range r^{-8} or r^{-12} repulsive potential should dominate at high temperatures. Mason found that up to 2000°K and Dukowicz found that up to 5000°K the reduced potential K_o was in the neighborhood of 4 cm^2/v-sec. Hence, the potential at a density ρ is

$$K = K_o \frac{\rho_o}{\rho} = 4\,\rho_o/\rho \quad \frac{cm^2}{v\text{-sec}} \qquad (29)$$

where ρ_o is the standard density of air.

Their calculations are restricted to low electric fields so

$$E/P \ll 2 \quad \frac{\text{volts}}{\text{cm-mm Hg}} \qquad (30)$$

If the above condition is violated then the ion drift velocity v_d is no longer simply proportional to the electric field.

Calculations at 270 Kft using the results shown in Fig. 23 indicate that inequality (30) is not satisfied throughout the sheath even if the sheath fills the boundary layer. For a sheath thickness of 1 cm at s = .37 ft, E(0)/P = 7.8 volts/cm-mm Hg. Similar conclusions are reached for other altitudes for sheath thicknesses like those shown in Fig. 21. Hence, the mobility-limited drift relation is not valid strictly speaking. But, it still should provide a first approximation to the ion drift velocity since E/P will be less than 2 volts/cm-mm Hg over much of the sheath even if it exceeds this value at the wall.

IV. CONCLUSIONS

1. Except for current traces associated with those probes located on the nose cap at 270 Kft, the experimental results were bound from above by the total convective current in the boundary layer and from below by the Q-1-D or diffusion currents.

2. Since the experimental currents on the nose region at 270 Kft are larger than the total currents being convected through the boundary layer, the predicted ion number densities are probably too low.

3. In the regions where convective effects are important, the ion sheath structure is too complex to properly describe by simple theories. One must use numerical methods to adequately describe the flow field.

4. At 270 Kft, on the conical portion of the vehicle, it appears that the inclusion of convective effects using the Q-1-D theory can explain the experimental results.

5. At no altitude between 220 Kft and 270 Kft on the nose, did either simple convection or diffusion theories produce results consistent with the data. But, it appears that an enhanced diffusion current due to local charge depletion in the boundary layer near the outer edge of the sheath may be sufficient to explain the experimental results. More effort is required to clarify this point.

Appendix

Description of Load Line Program

Card #

1 Title 80 columns

2 Te(^{o}K), $u_e(\frac{cm}{sec})$, V_w (value), FACRHØ, FACY, NY, NYS (5F10.0,2I5)

$$FACRHØ = \begin{cases} 1 \text{ if density table is gm/cm}^3 \\ .551 \text{ if density table is slug/ft}^3 \end{cases}$$

$$FACY = \begin{cases} 1 \text{ if y table is in cm} \\ 30.48 \text{ if y table is in ft} \end{cases}$$

NY = number of table entries (30 typically)

NYS = number (odd) intervals to compute sheath properties (i.e., boundary layer is divided into NYS strips)

NY Cards

y, ρ, $\theta = \frac{T}{T_e}$; $N_e(\frac{\#}{cm})$, $\frac{u}{u_e}$, (5F 12.0)

YS, NYPR (F10.0,I5)

YS = y_{sheath} = original sheath thickness in cm (just less than $y_{b.l.}$)

NYPR = number of printout station through sheath (odd).

Units are c.g.s.

LOAD LINE PROGRAM

```
LEVEL 17 ( 1 NOV 68)                OS/360  FORTRAN H                              DATE  72.153/10.41.07

        COMPILER OPTIONS - NAME= MAIN,OPT=00,LINECNT=50,SOURCE,BCD,NOLIST,DECK,LOAD,MAP,NOEDIT,ID,NOXREF
  ISN 0002              IMPLICIT REAL*8(A-H,O-Z),(INTEGER(I-N)
                  C     SPECIAL FOR R.J.
  ISN 0003              DIMENSION Y(5),F(5),ER(5),REL(5),SY(5),YI(100),RHOI(100),ED(100),
                      1           FP(100),THETA(100),DEODY(100),SA(15,100),SAS(4,100),
                      2           TITLE(80)
  ISN 0004              LOGICAL*1 TITLE
  ISN 0005          250 READ(5,254) (TITLE(I),I=1,80)       no of input V vls at which ρ, Ni, etc given
  ISN 0006          254 FORMAT(80A1)
  ISN 0007              READ(5,1) TE,UE,VII,FACRHO,FACY,NY,NYS  → No of Y's at which want DZL computed
  ISN 0008            1 FORMAT(5F10.0,2I5)
  ISN 0009              READ(5,251) (YI(I),RHOI(I),THETA(I),ED(I),FP(I),I=1,NY)
  ISN 0010          251 FORMAT(5F12.0)
  ISN 0011              DO 256 I=1,NY
  ISN 0012              YI(I)=YI(I)*FACY            }  TO CONVERT  INPUT TABLE  IN CASE  Y  NOT IN cm OR
  ISN 0013          256 RHOI(I)=RHOI(I)*FACRHO      }                                   RHO NOT IN gms/cm³
  ISN 0014              READ(5,252) YS,NYPR
  ISN 0015          252 FORMAT(F10.0,I5)
  ISN 0016              DYS=YS/DFLOAT(NYS)    increment by which sheath size stepped down
  ISN 0017              YS=YS+DYS
  ISN 0018          253 NYS=NYS-1
  ISN 0019              IF(NYS.LT.0) GO TO 250
  ISN 0021              YS=YS-DYS
  ISN 0022              DYPR=YS/DFLOAT(NYPR-1)   interval at which vls. are to be printed out
  ISN 0023   Ṽ^{2/3} =  Y(1)=0.0D0    } initial vls for V and E at outer edge of sheath
  ISN 0024   E²      =  Y(2)=0.0D0    }
  ISN 0025              YY=YS
  ISN 0026              DY=-1.0D-06   initial Δy (negative cause are stepping in from sheath)
  ISN 0027              SY(1)=Y(1)   } save initial vls for
  ISN 0028              SY(2)=Y(2)   } V(y₁), E(y₁)
  ISN 0029              SYY=YY        save initial vl for Y
  ISN 0030              K=2
  ISN 0031              M=1
  ISN 0032              L=0
  ISN 0033              IN=1
  ISN 0034              KH=0
  ISN 0035              YPR=YS      FIRST PRINT STATION IS YS
  ISN 0036              SDY=DY      save initial DY
  ISN 0037           50 CALL GETRHO(YY,YI,RHOI,RHO,NY,IERR)   Call Lagrangian 3-pt. interpolation subroutine to obtain interpolated
                                                                                                          vls. for RHO
  ISN 0038              GO TO (20,10),IERR
  ISN 0039           20 F(2)=-2.2830D15*RHO                              F(2) = dE²/dy
  ISN 0040              E=-DSQRT(Y(2))
  ISN 0041              IF(Y(1).NE.0.0D0) GO TO 25
  ISN 0043              BV=0.0D0
  ISN 0044              F(1)=(-4.0D0*F(2)/9.0D0)**(1.0D0/3.0D0)  =  (dṼ^{2/3}/dy)_{y=y₁}
  ISN 0045              GO TO 32
  ISN 0046           25 BV=-(-Y(1))**1.5D0   = Ṽ
  ISN 0047              BV1=DSQRT(-Y(1))
  ISN 0048              F(1)=-2.0D0*E/BV1/3.0D0  =  dṼ^{2/3}/dy
```

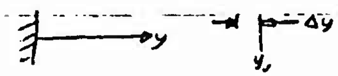

```
                        ISN 0049      32 GO TO (30,40),K
                        ISN 0050      30 K=MERKUT(2,Y,F,ER,YY,DY,H)
Using MERKUT            ISN 0051         GO TO 50                        If IN = 1, GO TO 60
subroutine              ISN 0052      40 GO TO (60,70),IN                "  "  = 2  "   "  70
(Runge-Kutta            ISN 0053      60 IN=2
3rd scheme)             ISN 0054      65 L=L+1
compute                 ISN 0055         SA(1,L)=YY
f(1), V(Y)              ISN 0056         SA(2,L)=BV = V~          L is indexing variable for Y and dependent variables
                        ISN 0057         SA(3,L)=E  = E~          goes from 1 to NYPR
                        ISN 0058         SA(4,L)=RHO
                        ISN 0059         IF(DABS(SDY).GE.DYPR) SDY=-DYPR/2.4D0   - to keep Dy < Δy print
                        ISN 0061         DY=SDY
                        ISN 0062         YPR=YPR-DYPR
                        ISN 0063         IF(L.EQ.NYPR) GO TO 150
                        ISN 0065         GO TO 30
                        ISN 0066      70 DO 80 I=1,2
                        ISN 0067         IF(Y(I).EQ.0.0D0) GO TO 75
                        ISN 0069         REL(I)=DABS(ER(I)/Y(I))          Computing % error in E~^2 and V~^2/3
                        ISN 0070         GO TO 80
                        ISN 0071      75 REL(I)=0.0D0
                        ISN 0072      80 CONTINUE
                        ISN 0073         IF(REL(1).GT.1.0D-05) GO TO 90
                        ISN 0075         IF(REL(2).GT.1.0D-05) GO TO 90
                        ISN 0077         IF(REL(1).GT.1.0D-07) GO TO 100
                        ISN 0079         IF(REL(2).GT.1.0D-07) GO TO 100
                        ISN 0081         DY=2.0D0*DY
                        ISN 0082     100 SY(1)=Y(1)
                        ISN 0083         SY(2)=Y(2)
                        ISN 0084         SYY=YY
                        ISN 0085         KH=0
                        ISN 0086         IF(DABS(YY-YPR).LT.1.0D-10) GO TO 65
                        ISN 0088         SDY=DY
                        ISN 0089         IF(YY+DY.LT.YPR) DY=YPR-YY
                        ISN 0091         GO TO 30
                        ISN 0092      90 CONTINUE
                        ISN 0093         Y(1)=SY(1)       save old vls for E~^2 and V~^2/3
                        ISN 0094         Y(2)=SY(2)
                        ISN 0095         YY=SYY        save old vl for Y
                        ISN 0096         DY=DY/2.0D0     reduce step size in attempt to reduce relative error
                        ISN 0097         SDY=DY
                        ISN 0098         K=1
                        ISN 0099         KH=KH+1
                        ISN 0100         IF(KH.LE.10) GO TO 50    just half step size 10 times to reduce relative error to ≤ 1 part in 10^5
                        ISN 0102         WRITE(6,21)
                        ISN 0103      21 FORMAT(25H CANT STEP AFTER 10 TRIES)    If can't cut down REL to < 10^5 after 10 tries, call exit
                        ISN 0104      10 CALL EXIT
                        ISN 0105     150 DO 155 I=1,L
                        ISN 0106         DO 155 J=1,4
```

If NYPR = 5:

L = 5 4 3 2 1 0

```
155 SAS(J,I)=SA(J,I)          Y, V, z, ρ
    DO 157 I=1,L
    II=L-I&1
    DO 157 J=1,4
157 SA(J,II)=SAS(J,I)
    SUM=0.0D0
    C1=DYPR/3.0D0
    LM2=L-2
    DO 120 I=1,LM2,2
120 SUM=SUM&C1*(SA(4,I)&4.0D0*SA(4,I&1)&SA(4,I&2))  } compute av. vl of ρ = RHOBAR
    RHOBAR=SUM/YS
    S2J=-VW/SA(2,1)
    DO 175 I=1,L
    DO 175 J=2,3
175 SA(J,I)=SA(J,I)*S2J
    BJLLCO=4.95D-16*VW**2/YS**3/RHOBAR   approx current assuming constant density
    BJLL=S2J**2/2.0D0   actual load line current
    SA(5,1)=THETA(1)
    SA(6,1)=ED(1)
    SA(7,1)=FP(1)
    LM1=L-1
    DO 140 I=2,L
    YY=SA(1,I)
    CALL GETRHO(YY,YI,THETA,ANS,NY,IERR)
    GO TO (132,10),IERR
132 SA(5,I)=ANS                Using GETRHO SUBROUTINE TO COMPUTE
    CALL GETRHO(YY,YI,ED,ANS,NY,IERR)      THETA, ED, FP AT YPRINT CO-ORDI
    SA(6,I)=ANS
    CALL GETRHO(YY,YI,FP,ANS,NY,IERR)
140 SA(7,I)=ANS
    C1=1.6CD-19*UE
    DO 160 I=1,L
160 SA(8,I)=C1*SA(7,I)*SA(6,I)   = eNiui
    SA(9,1)=0.0D0
    C1=DYPR/3.0D0/.635D0
    C2=DYPR/12.0D0/.635D0
    DO 170 I=1,LM2,2
    SA(9,I&1)=SA(9,I)&C2*(5.0D0*SA(8,I)&8.0D0*SA(8,I&1)-SA(8,I&2))
170 SA(9,I&2)=SA(9,I)&C1*(SA(8,I)&4.0D0*SA(8,I&1)&SA(8,I&2))   = 1/wp ∫_0^ypr eu:Ni dy
    C3=2.0D0*DYPR
    DEDDY(1)=(-3.0D0*SA(6,1)&4.0D0*SA(6,2)-SA(6,3))/C3
    DEDDY(L)=(SA(6,LM2)-4.0D0*SA(6,LM1)&3.0D0*SA(6,L))/C3
    DO 180 I=2,LM1
180 DEDDY(I)=(SA(6,I&1)-SA(6,I-1))/C3 - central difference to compute dNe/dy
    C4=1.37D-25*TE
    DO 190 I=1,L
190 SA(10,I)=C4*SA(5,I)*DEDDY(I)/SA(4,I) = jd
    WRITE(6,2011) (TITLE(I),I=1,80)
```

```
ISN 0155      201 FORMAT(1H1,1X80A1)
ISN 0156          WRITE(6,202) VH,TE,UE,RHODAR,BJLLCD,BJLL,YS
ISN 0157      202 FORMAT(2X3HVH=E13.5,2X3HTE=E13.5,2X3HUE=E13.5,2X5HRHOB=E13.5,
                 1       2X6HJLLCD=E13.5,2X4HJLL=E13.5,2X3HYS=E13.5/6X1HY,12X1HV,
                 2       12X1HE,10X3HRHO,0X5HTHETA,11X2HNE,9X4HU/UE,10X3HCJD,
                 3       11X2HCJ,9X4HCJDR)
ISN 0158          DO 210 I=1,L
ISN 0159      210 WRITE(6,211) (SA(J,I),J=1,10)
ISN 0160      211 FORMAT(10E13.5)
ISN 0161          GO TO 253
ISN 0162          END
ADCONS FOR EXTERNAL REFERENCES
```

```
        COMPILER OPTIONS - NAME=  MAIN,OPT=00,LINECNT=50,SOURCE,BCD,NOLIST,DECK,LOAD,MAP,NOEDIT,ID,NOXREF
ISN 0002         IMPLICIT REAL*8(A-H,O-Z),(INTEGER(I-N)
ISN 0003         SUBROUTINE GETRHO(YY,Y,R,RHO,N,IERR)
ISN 0004         DIMENSION Y(100),R(100)
ISN 0005         DO 10 I=1,N
ISN 0006         IF(Y(I).GE.YY) GO TO 20
ISN 0008      10 CONTINUE
ISN 0009         WRITE(6,1)
ISN 0010       1 FORMAT(25H Y OUT OF TABLE IN GETRHO)
ISN 0011         IERR=2
ISN 0012         RETURN
ISN 0013      20 IF(I.EQ.N) I=N-1
ISN 0015         IF(I.EQ.1) I=2
ISN 0017         IM1=I-1
ISN 0018         IP1=I+1
ISN 0019         Y1=Y(IM1)
ISN 0020         Y2=Y(I)
ISN 0021         Y3=Y(IP1)
ISN 0022         V1=(YY-Y2)*(YY-Y3)/(Y1-Y2)/(Y1-Y3)
ISN 0023         V2=(YY-Y1)*(YY-Y3)/(Y2-Y1)/(Y2-Y3)
ISN 0024         V3=(YY-Y1)*(YY-Y2)/(Y3-Y1)/(Y3-Y2)
ISN 0025         RHO=V1*R(IM1)&V2*R(I)&V3*R(IP1)
ISN 0026         IERR=1
ISN 0027         RETURN
ISN 0028         END
```

R is 3rd entry space in GETRHO subroutine and can be whatever we want it to be like ρ_o, M_1, etc

Here we say R = RHO

YY = Y

YY is tabulated given val

Y(I) is interpolated val.

```
COMPILER OPTIONS - NAME=  MAIN,OPT=00,LINECNT=50,SOURCE,BCD,NOLIST,DECK,LOAD,MAP,NOEDIT,ID,NOXREF
ISN 0002          IMPLICIT REAL*8(A-H,O-Z),INTEGER(I-N)
ISN 0003          FUNCTION MERKUT(N,Y,F,ER,X,H,M)
ISN 0004          DIMENSION Y(20),F(20),ER(20),Y1(20),FK1(20),FK2(20),FK3(20),
                1      FK4(20),FK5(20)
ISN 0005          GO TO (10,20,30,40,50),M
ISN 0006       10 HO3=H/3.0D0
ISN 0007          HO2=H/2.0D0
ISN 0008          HO6=H/6.CD0
ISN 0009          DO 15 I=1,N
ISN 0010          Y1(I)=Y(I)
ISN 0011          FK1(I)=HO3*F(I)
ISN 0012       15 Y(I)=Y1(I)&FK1(I)
ISN 0013          X=X&HO3
ISN 0014          GO TO 80
ISN 0015       20 DO 25 I=1,N
ISN 0016          FK2(I)=HO3*F(I)
ISN 0017       25 Y(I)=Y1(I)&.500*(FK1(I)&FK2(I))
ISN 0018          GO TO 80
ISN 0019       30 DO 35 I=1,N
ISN 0020          FK3(I)=HO3*F(I)
ISN 0021       35 Y(I)=Y1(I)&.37500*(FK1(I)&3.000*FK3(I))
ISN 0022          X=X&HO6
ISN 0023          GO TO 80
ISN 0024       40 DO 45 I=1,N
ISN 0025          FK4(I)=HO3*F(I)
ISN 0026       45 Y(I)=Y1(I)&1.500*(FK1(I)-3.000*FK3(I)&4.000*FK4(I))
ISN 0027          X=X&HO2
ISN 0028          GO TO 80
ISN 0029       50 DO 55 I=1,N
ISN 0030          FK5(I)=HO3*F(I)
ISN 0031          Y(I)=Y1(I)&.500*(FK1(I)&4.0D0*FK4(I)&FK5(I))
ISN 0032       55 ER(I)=.200*FK1(I)-.9D0*FK3(I)&.800*FK4(I)-.100*FK5(I)
ISN 0033       77 M=1
ISN 0034          MERKUT=2
ISN 0035          RETURN
ISN 0036       80 M=M&1
ISN 0037          MERKUT=1
ISN 0038          RETURN
ISN 0039          END
```

N ... M are variables upon which Merkut depends

Go TO 10 ... 50 depending on whether $M = 1, 2, \cdots 5$

$F(1) = \frac{d\tilde{V}^{1/2}}{dy}$ $F(2) = \frac{d\tilde{E}^2}{dy}$ $FK1(1) = \Delta\tilde{V}^{1/2}$ in interval HO3 $FK2(2) = \Delta\tilde{E}^2$ " " HO3

computing new vls for $\tilde{E}^2$ and $\tilde{V}^{1/2}$ at $Y+\Delta Y$ from vls at Y

Merson's adaption of Runge-Kutta 5th formula

computing ~~relative~~ absolute error in I^{st} vl.

REFERENCES

1. Hayes, D. T., "Electrostatic Probe Measurements of Flow Field Characteristics of a Blunt Body Reentry Vehicle," AIAA Paper #72-694, June 1972.

2. Lew, Henry, G., "Shock Layer Ionization at High Altitudes," (Final Report on Contract F19-628-69-C-0112), AFCRL-70-0702, GE 70SD782, The General Electric Co., Valley Forge, Pa. 19101, November 1970.

3. Bredfeldt, et al, "Boundary-Layer Ion Density Profiles as Measured by Electrostatic Probes," AIAA J. 5, January 1967, pp. 91-98.

4. Su, C. G., "Compressible Plasma Flow Over a Biased Body," AIAA J., 3, May 1965, pp. 842-848.

5. Dukowicz, J., "Theory of Convection-Conduction Dominated Electrostatic Probes: Numerical Solutions of the Two-Dimensional Flat Plate Problem," CAL Rep. No. RA-2641-Y-1, (1969).

6. Johnson, R. A. and deBoer, P. C. T., "Theory of Ion Boundary Layers," AIAA J., 10, May 1972, pp. 664-670.

7. Boyer, et al, "Experimental and Numerical Studies of Flush-Mounted Electrostatic Probes in Hypersonic Ionized Flows," AIAA 10th Aerospace Sciences Meeting, San Diego, Calif., January 1972.

8. Reilly, J., "Probe Data Verification," in "Research in Reentry Physics/ Final Technical Progress Report (U)," Doc. No. AERL 71-150 (December 1970), pp. 89-103, Secret.

9. deBoer, P. C. T. and Johnson, R. A., "Theory of Flat-Plate Ion-Density Probes," Phys. Fluids 11, 909-911 (1968).

10. Mason, E. A., "Estimated Ion Mobilities for Some Air Constituents," Planet Space Sci., 1970, 18, pp. 137-144.

11. Dukowicz, John, "Mobility of NO^+ Ions in Air," AIAA J, 8, April 1970, pp. 827-828.

FIG. 1. MEASURED CURRENT J_{exp} VS. ALTITUDE z

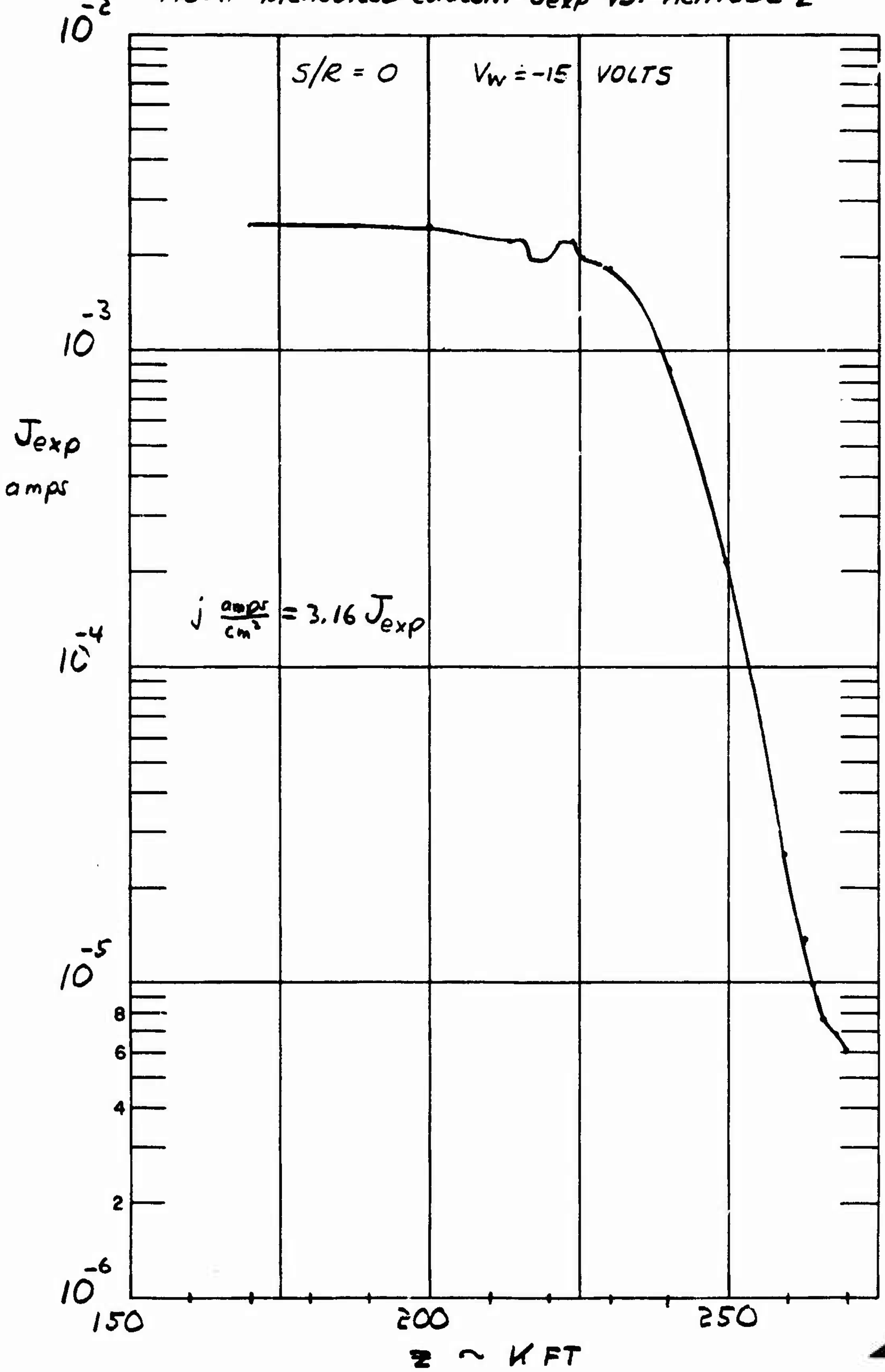

FIG. 2 MEASURED CURRENT J_{exp} VS. ALTITUDE Z

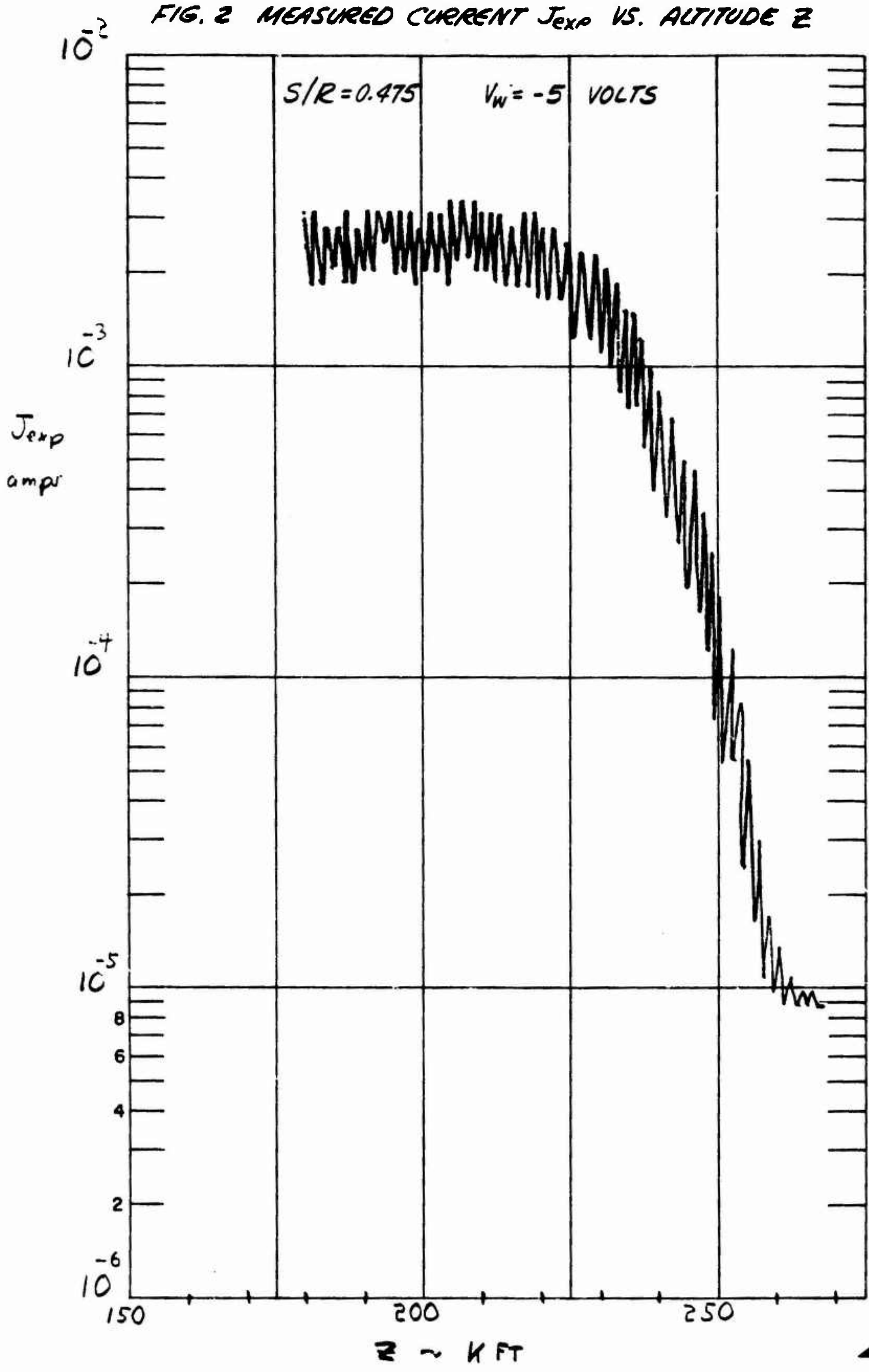

FIG. 3 MEASURED CURRENT J_{exp} VS. ALTITUDE z

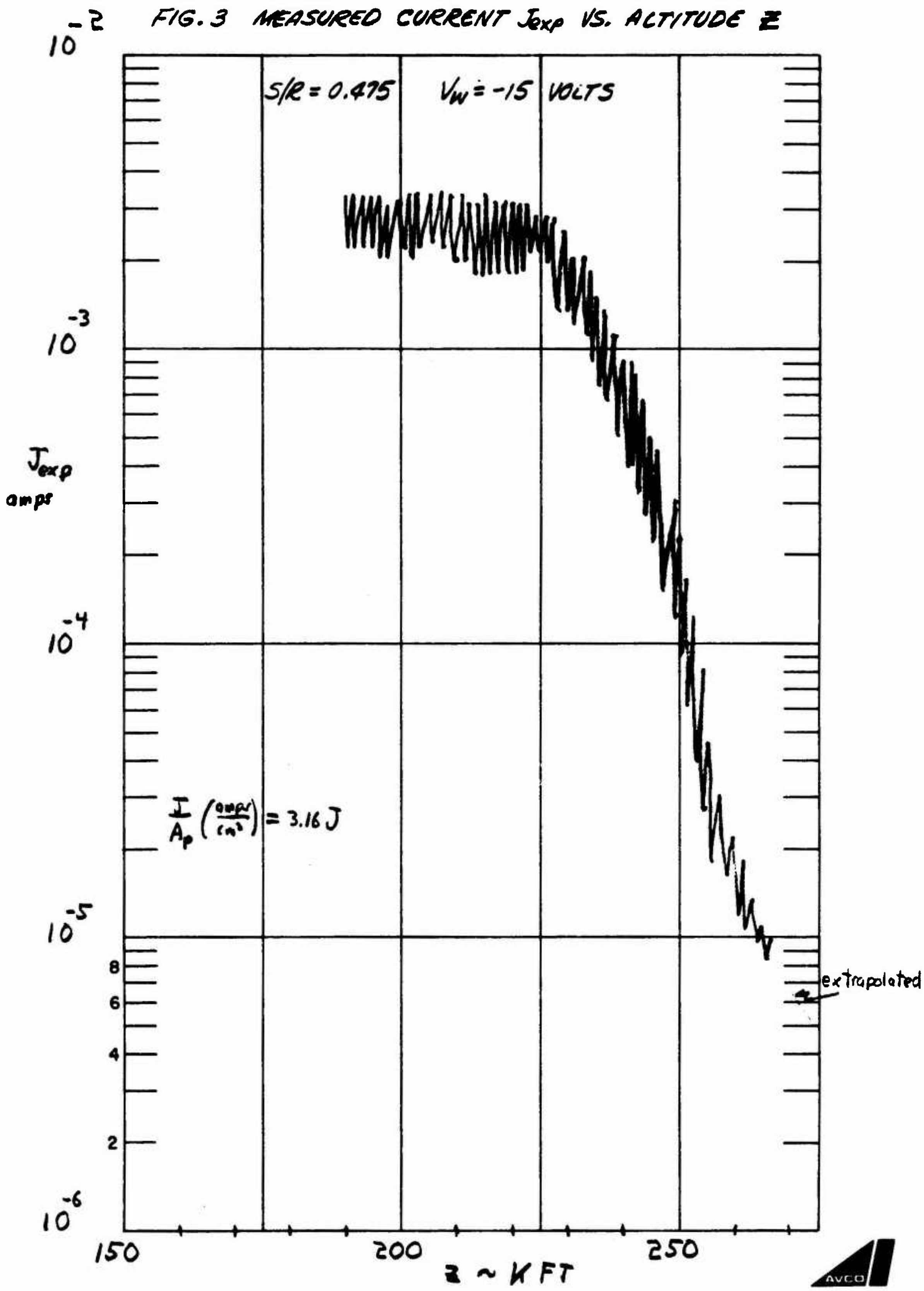

FIG. 4 MEASURED CURRENT J_{exp} VS. ALTITUDE Z

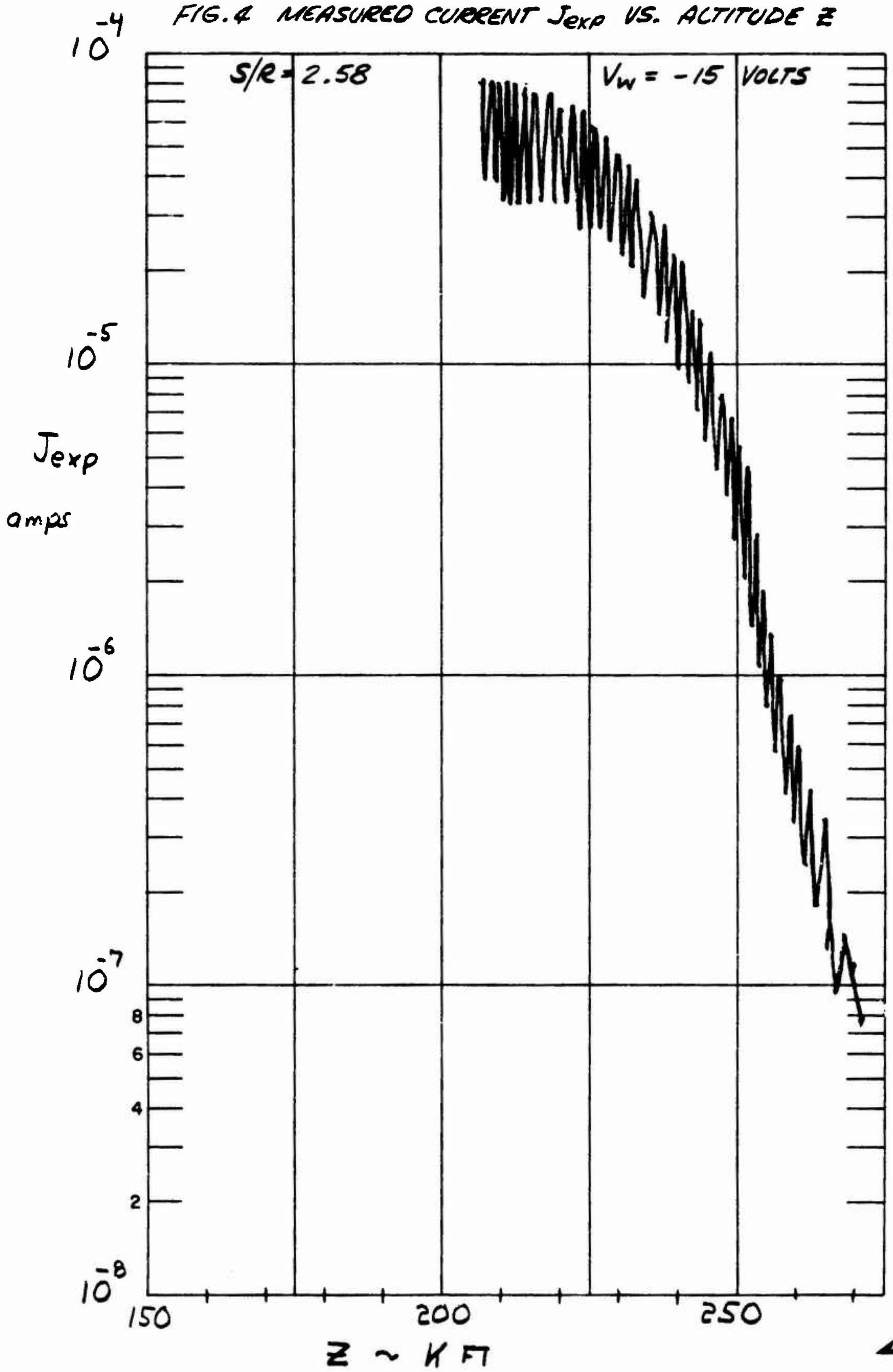

FIG. 5 SCHEMATIC SHOWING LATERAL VARIATION OF SHEATH HEIGHT

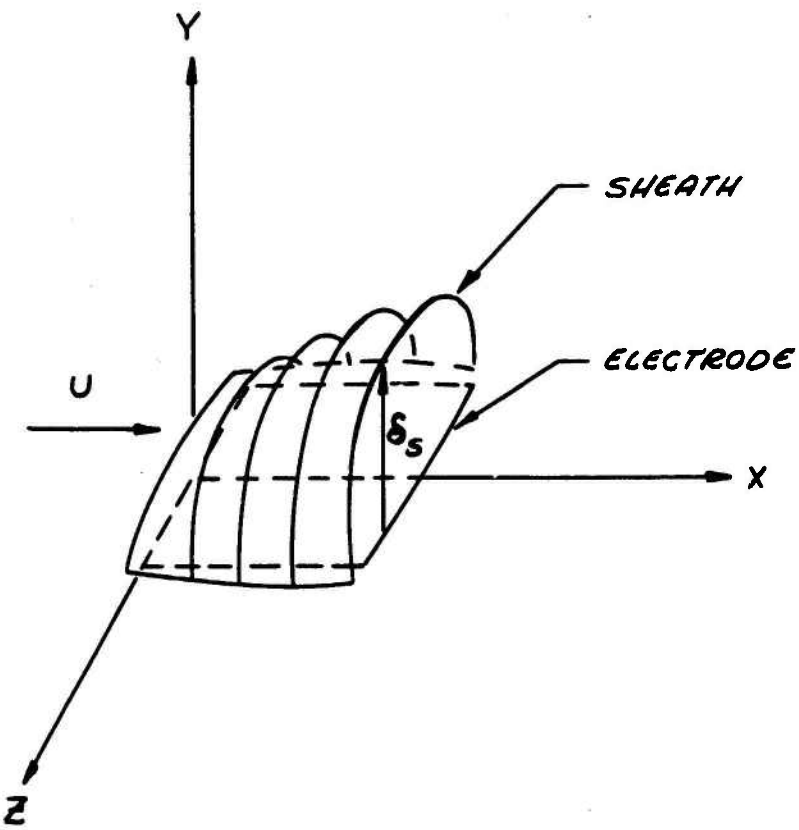

FIG. 6 SCHEMATIC OF CONVECTIVE CURRENT TO ELECTRODE, SHOWING SHEATH THICKNESS δ_s AND BOUNDARY LAYER THICKNESS $\delta_{b.l.}$

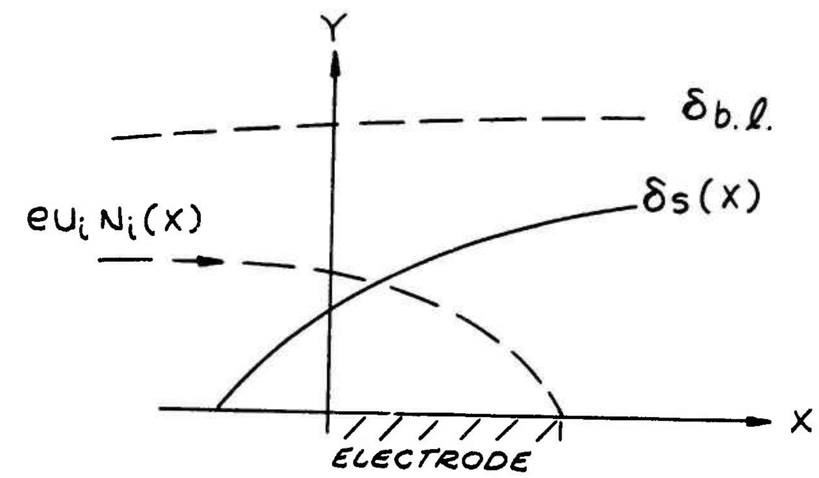

FIG. 7 COMPARISON BETWEEN MEASURED J_{exp} AND PREDICTED CURRENT DENSITIES

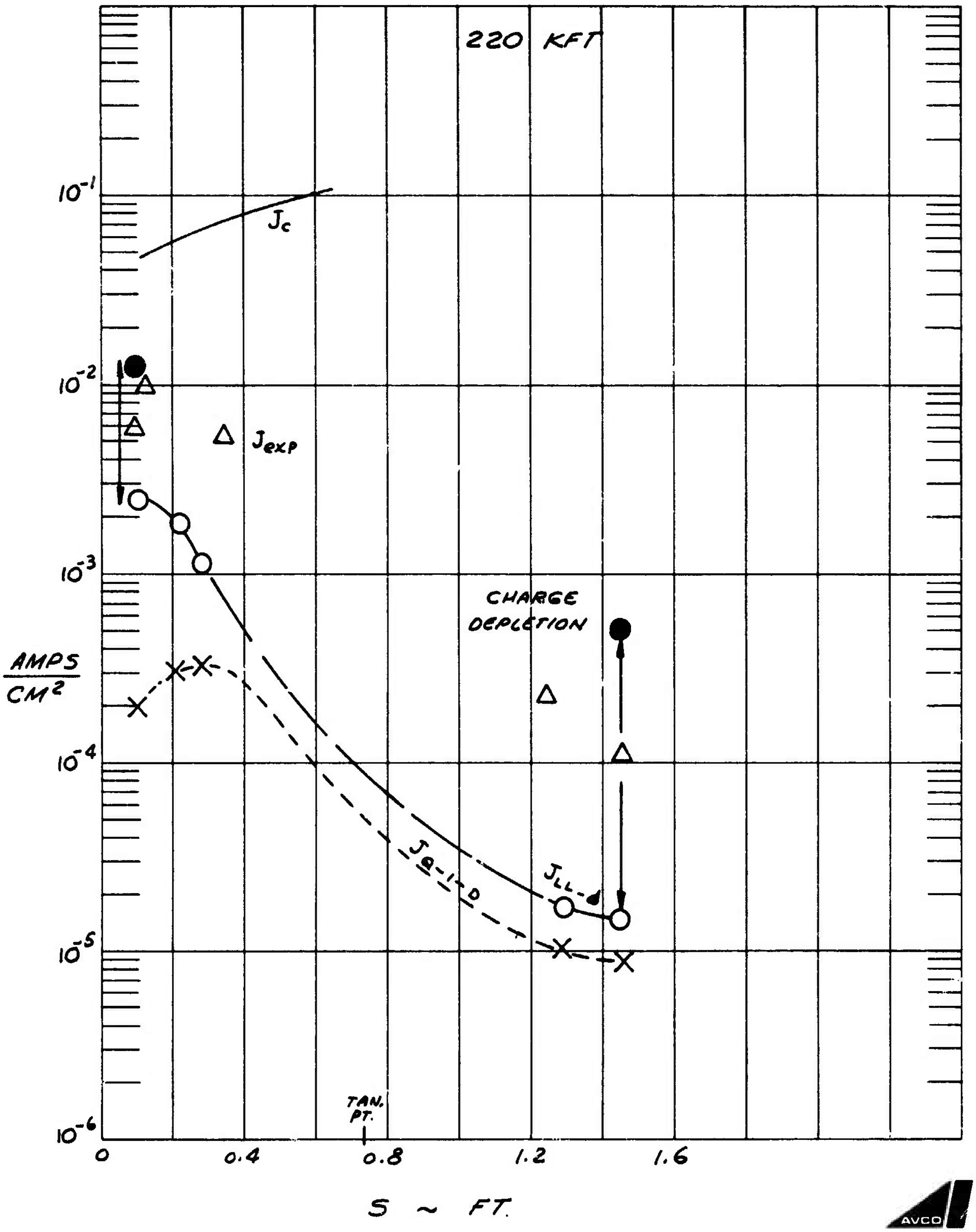

FIG. 8 COMPARISON BETWEEN MEASURED J_{exp} AND PREDICTED CURRENT DENSITIES

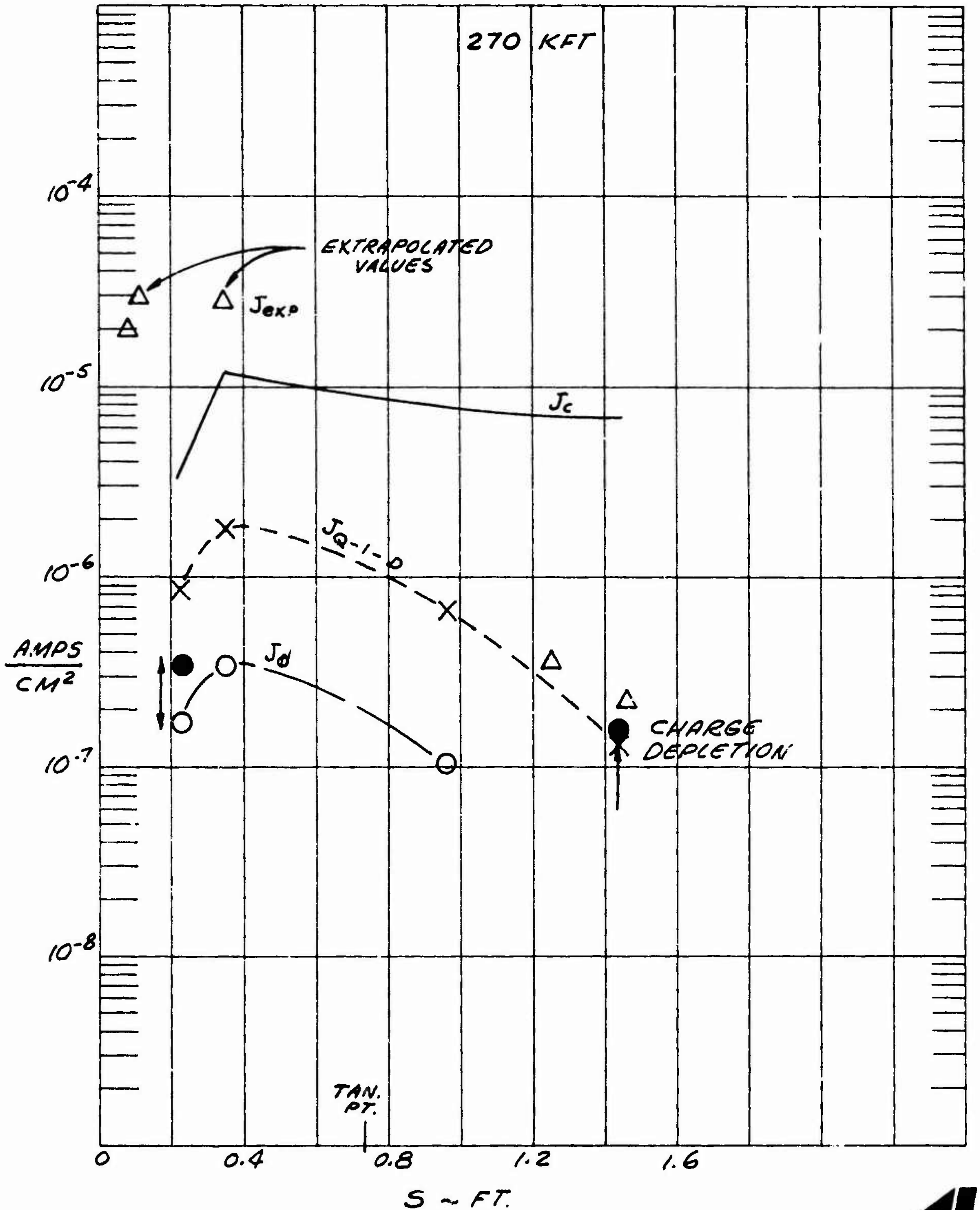

FIG. 9 COMPARISON BETWEEN MEASURED J_{exp} AND PREDICTED CURRENT DENSITIES

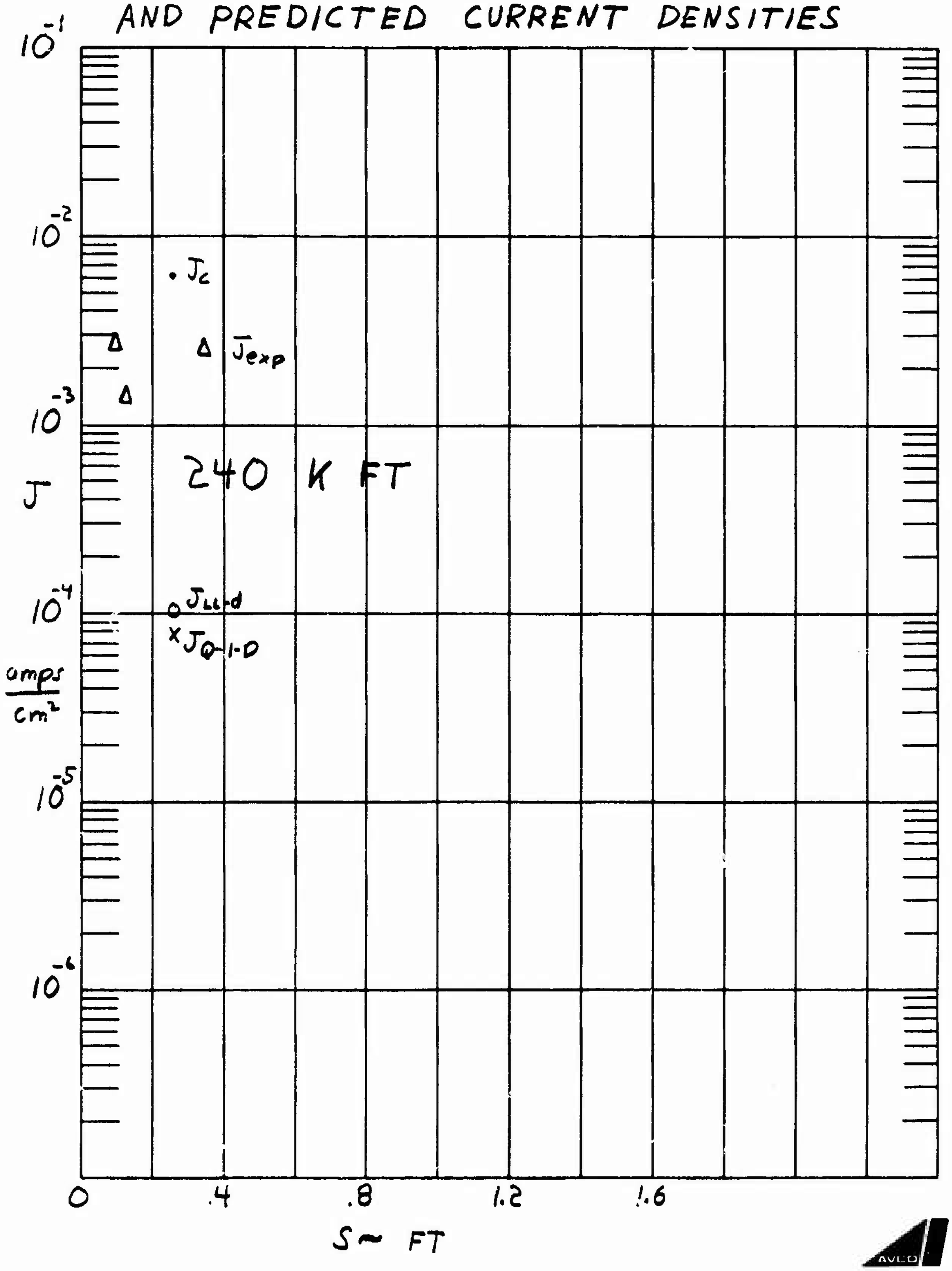

FIG. 10 THEORETICALLY PREDICTED CURRENT DENSITY J AS A FUNCTION OF DISTANCE FROM PROBE SURFACE y

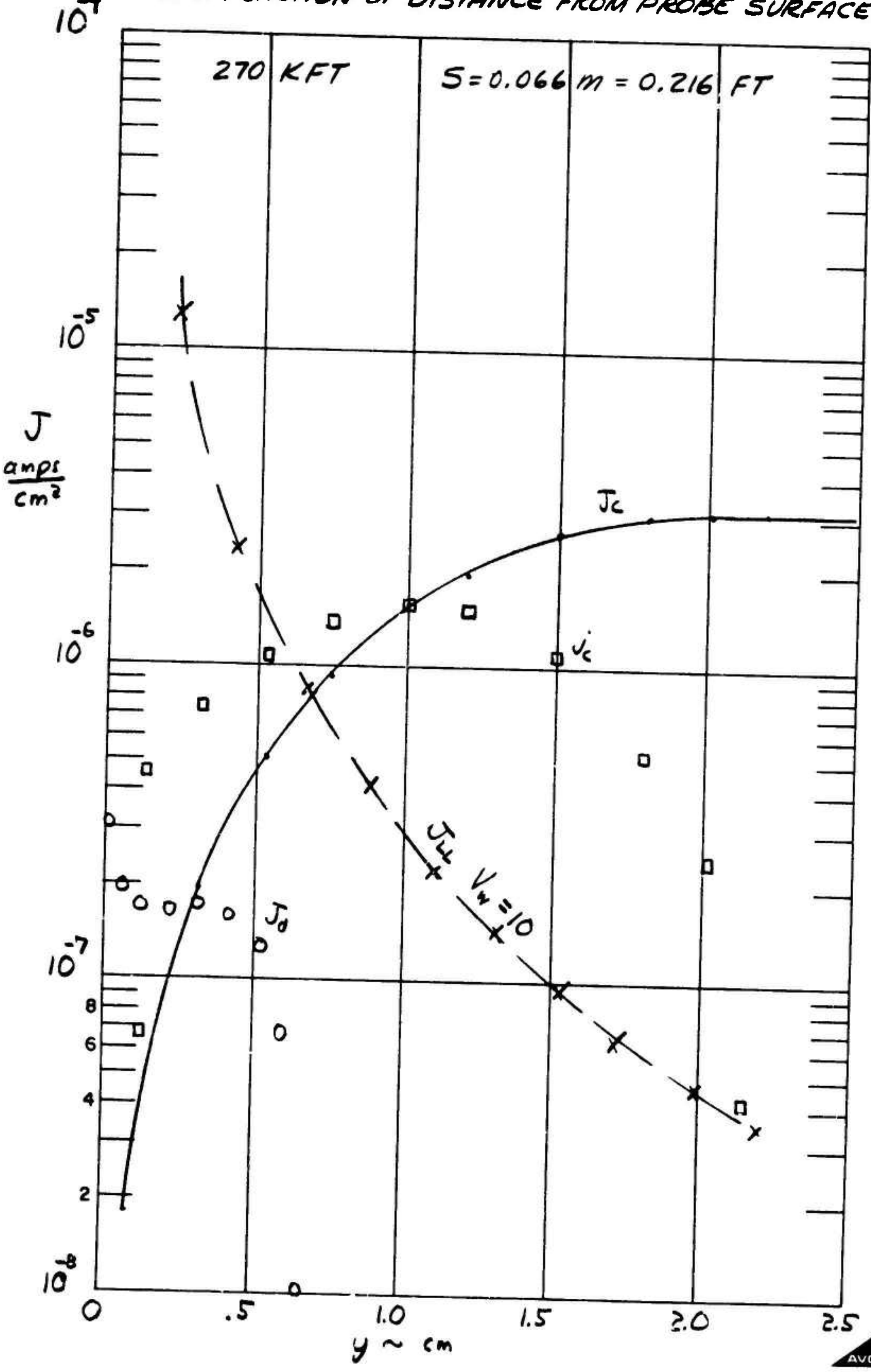

FIG. 11 THEORETICALLY PREDICTED CURRENT DENSITY J AS A FUNCTION OF DISTANCE FROM PROBE SURFACE y

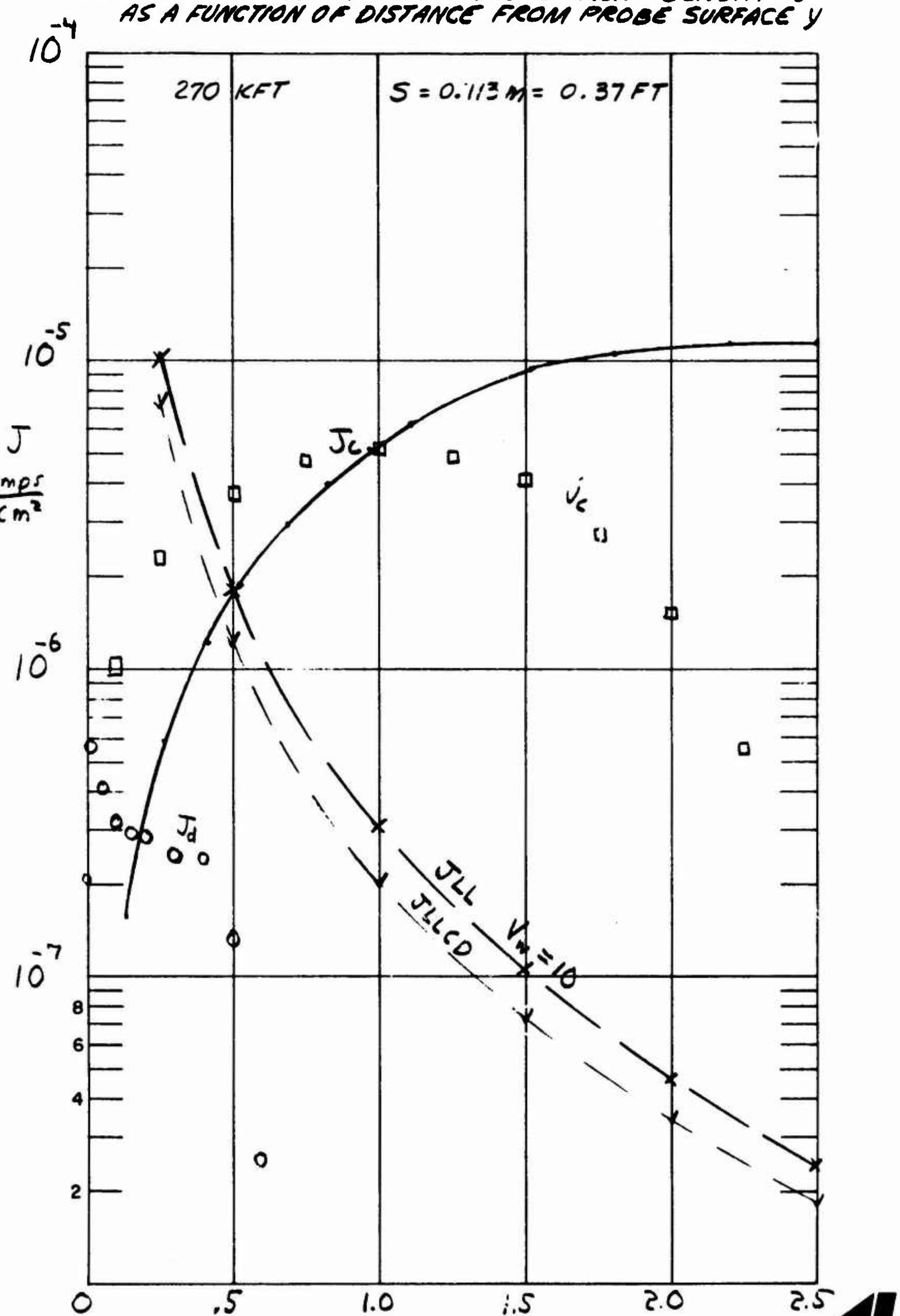

FIG. 12 THEORETICALLY PREDICTED CURRENT DENSITY J AS A FUNCTION OF DISTANCE FROM PROBE SURFACE y

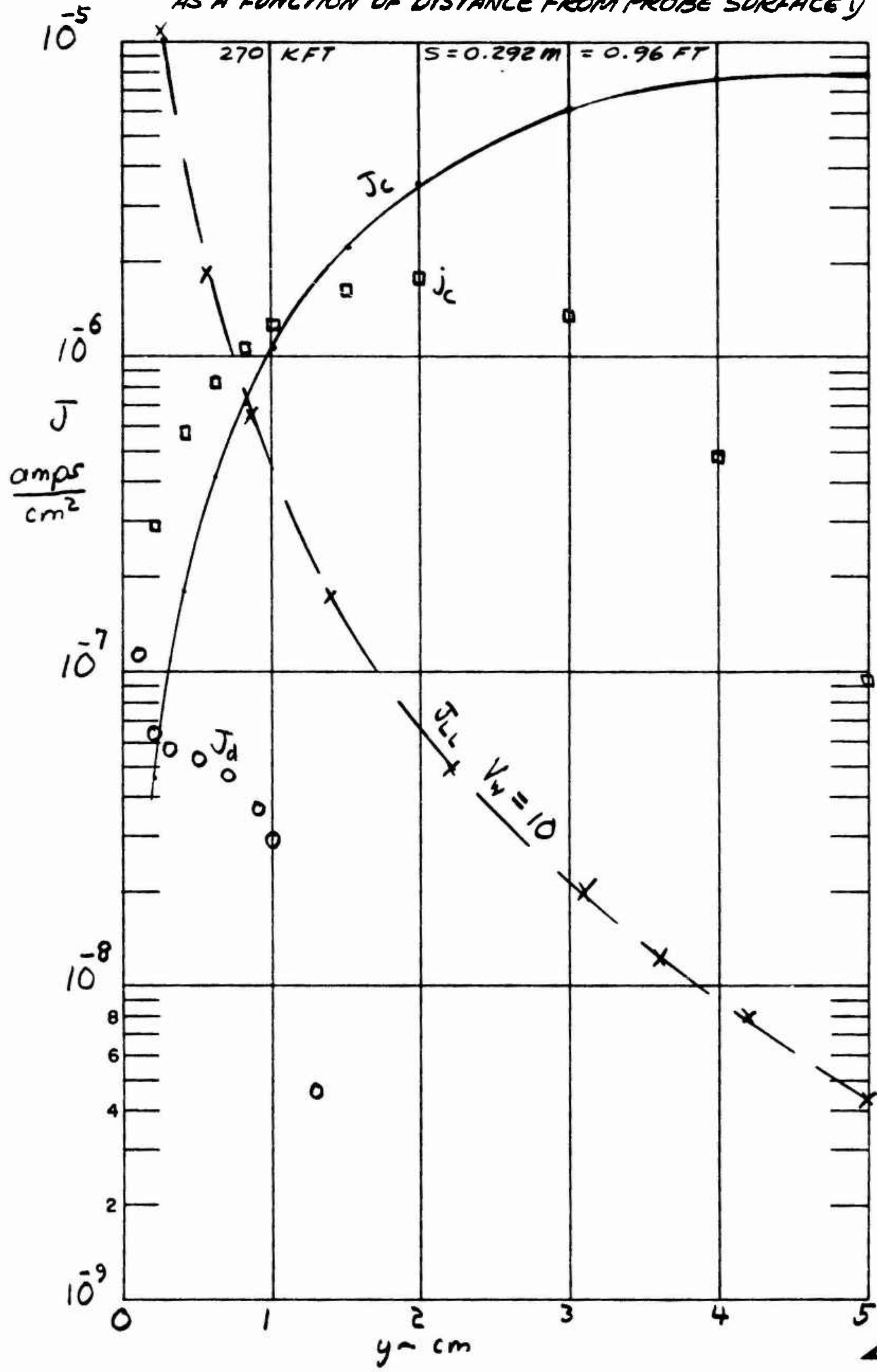

AVCO

FIG. 13 THEORETICALLY PREDICTED CURRENT DENSITY J AS A FUNCTION OF DISTANCE FROM PROBE SURFACE Y

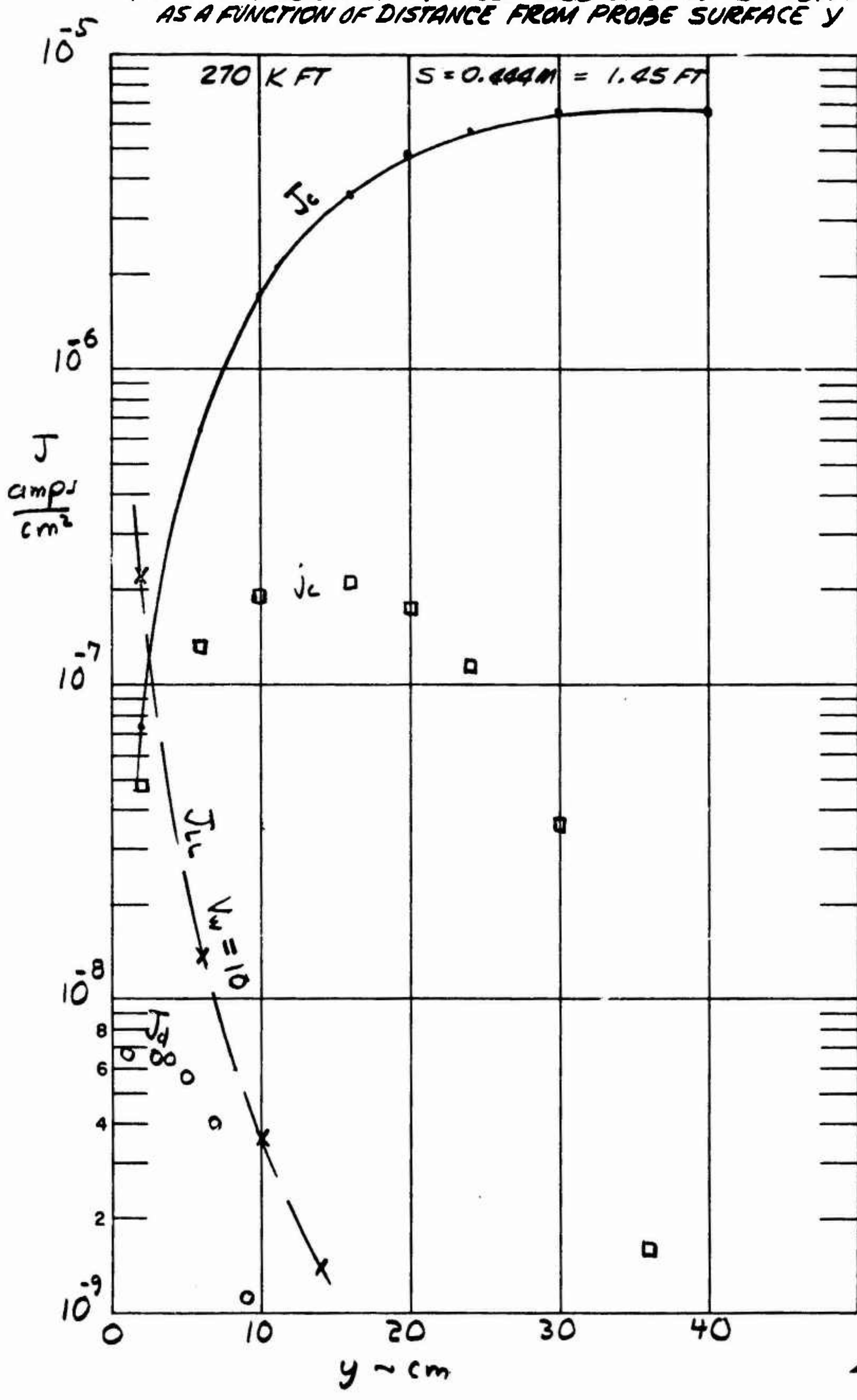

FIG. 14 THEORETICALLY PREDICTED CURRENT DENSITY J AS A FUNCTION OF DISTANCE FROM PROBE SURFACE y

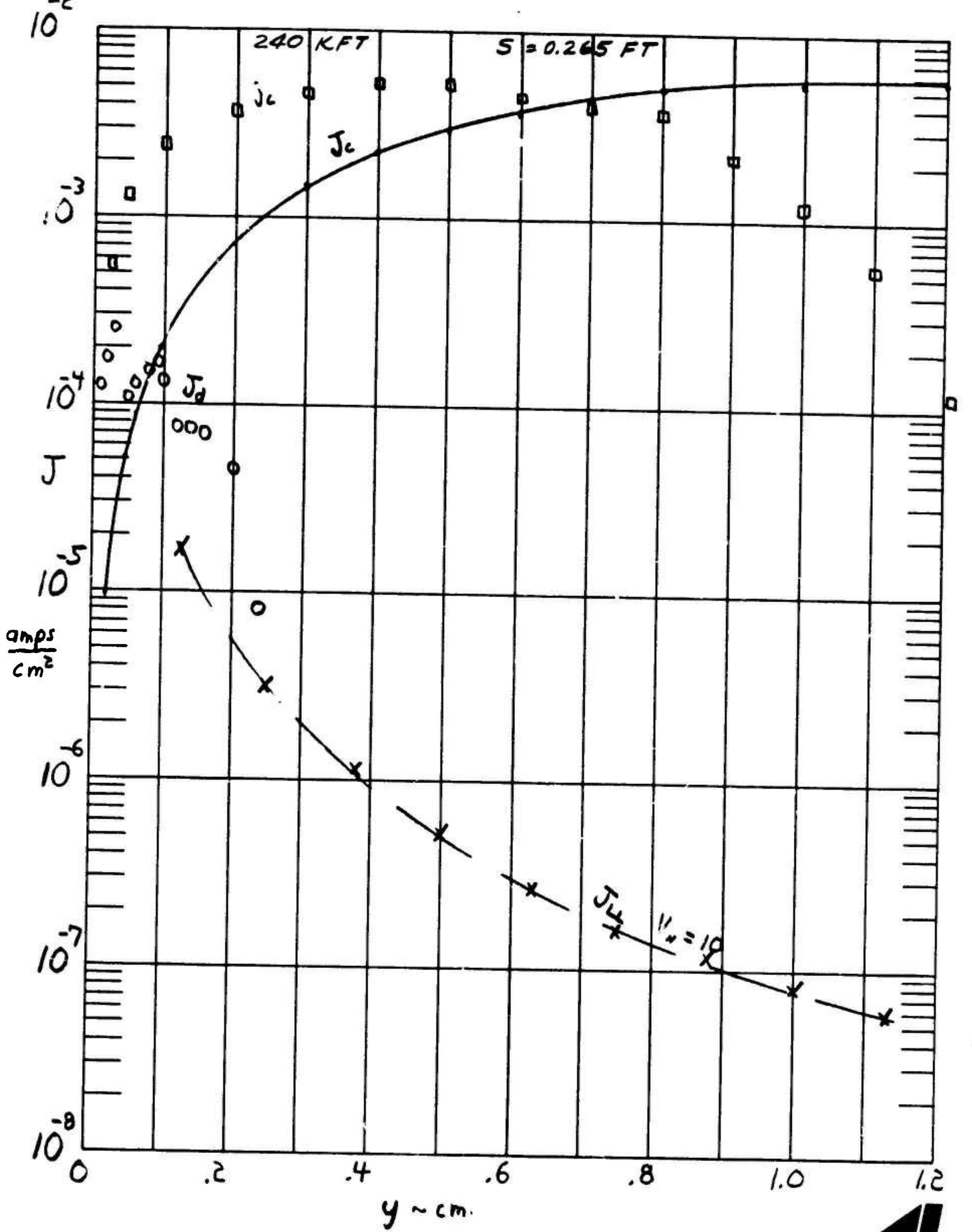

FIG. 15 THEORETICALLY PREDICTED CURRENT DENSITY J AS A FUNCTION OF DISTANCE FROM PROBE SURFACE Y

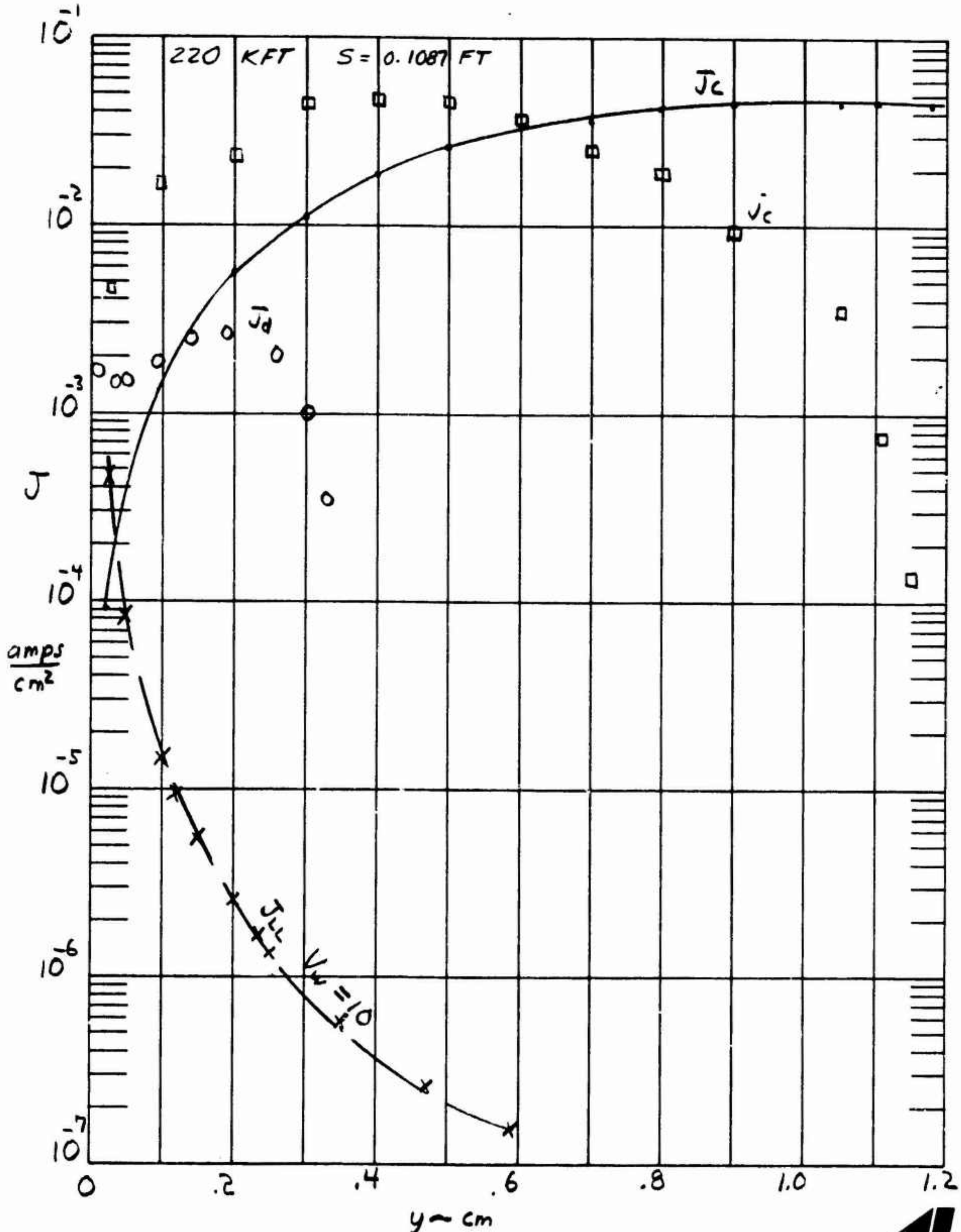

FIG. 16 THEORETICALLY PREDICTED CURRENT DENSITY J AS A FUNCTION OF DISTANCE FROM PROBE SURFACE y

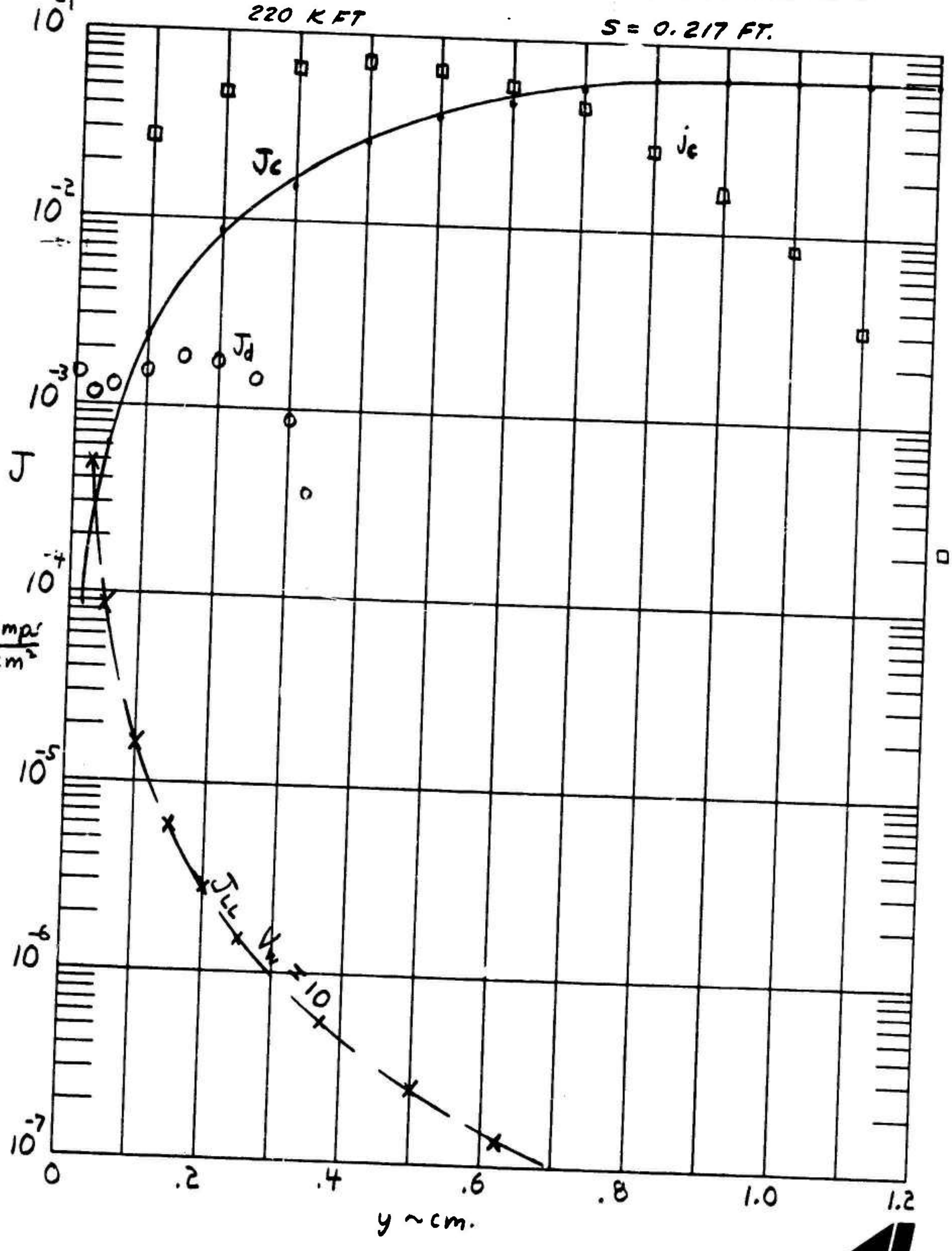

FIG. 17 THEORETICALLY PREDICTED CURRENT DENSITY J AS A FUNCTION OF DISTANCE FROM PROBE SURFACE y

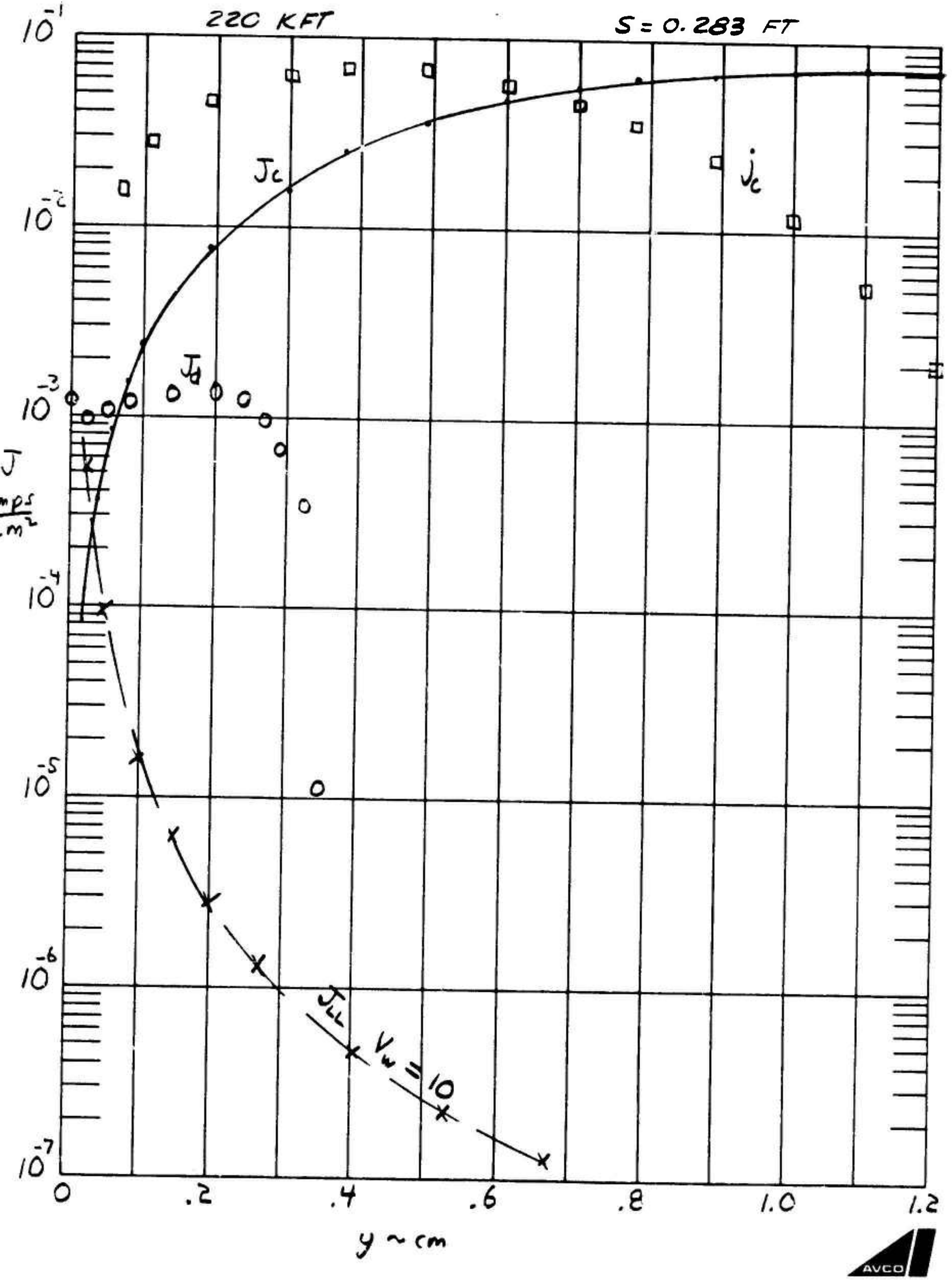

FIG. 18 THEORETICALLY PREDICTED CURRENT DENSITY J AS A FUNCTION OF DISTANCE FROM PROBE SURFACE y

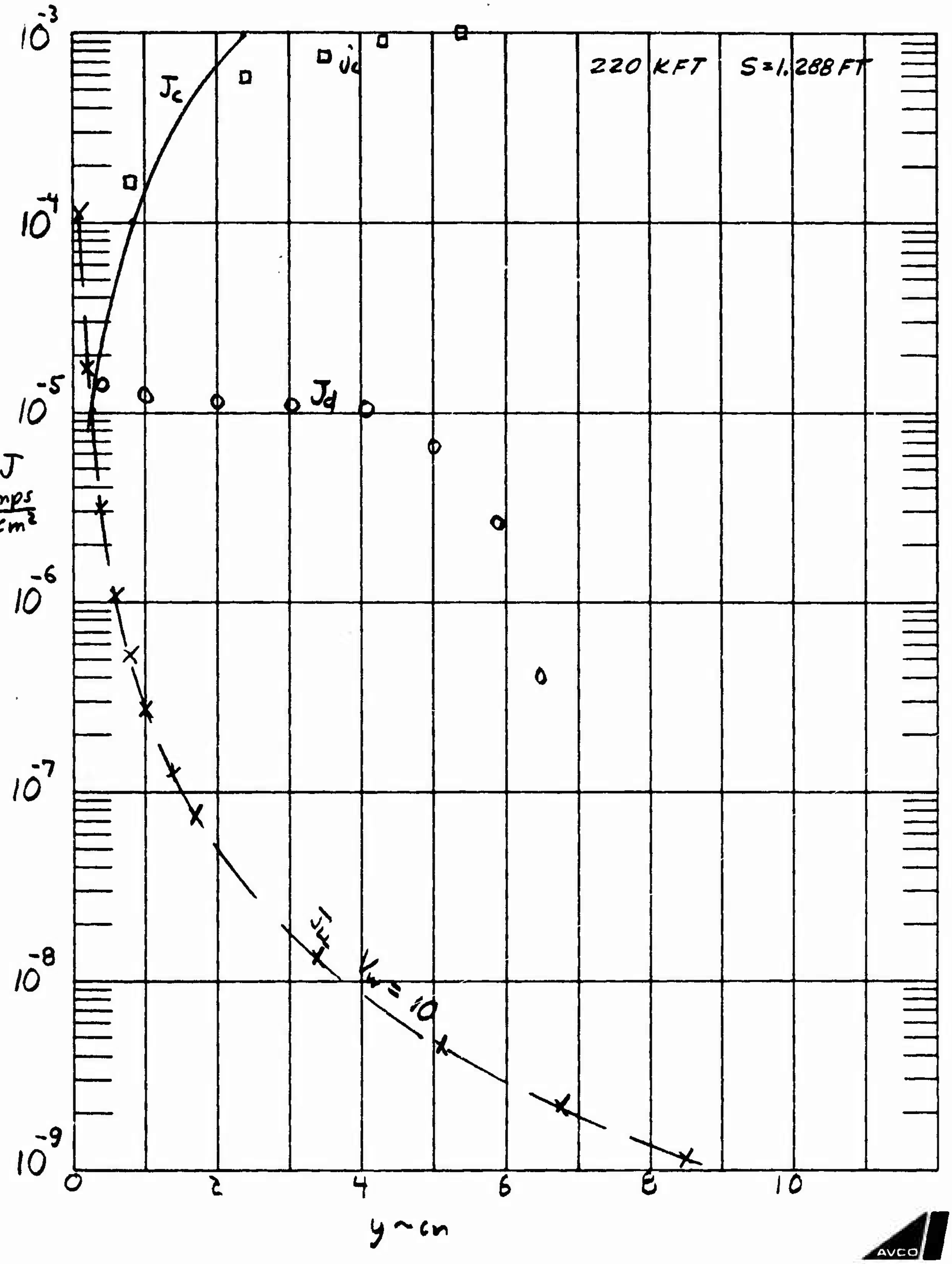

AVCO

FIG. 19 THEORETICALLY PREDICTED CURRENT DENSITY J AS A FUNCTION OF DISTANCE FROM PROBE SURFACE y

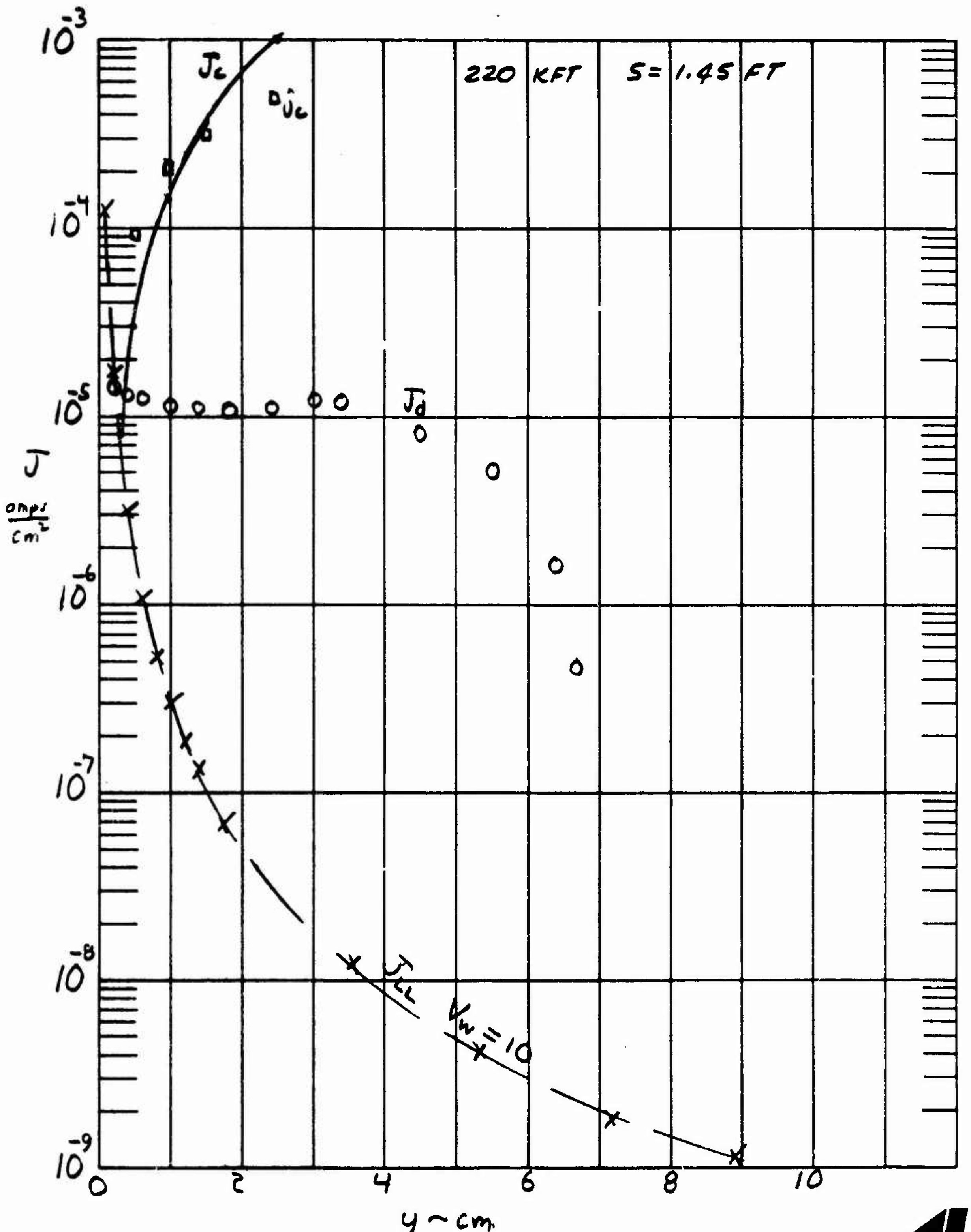

FIG. 20 FRINGING EFFECTS

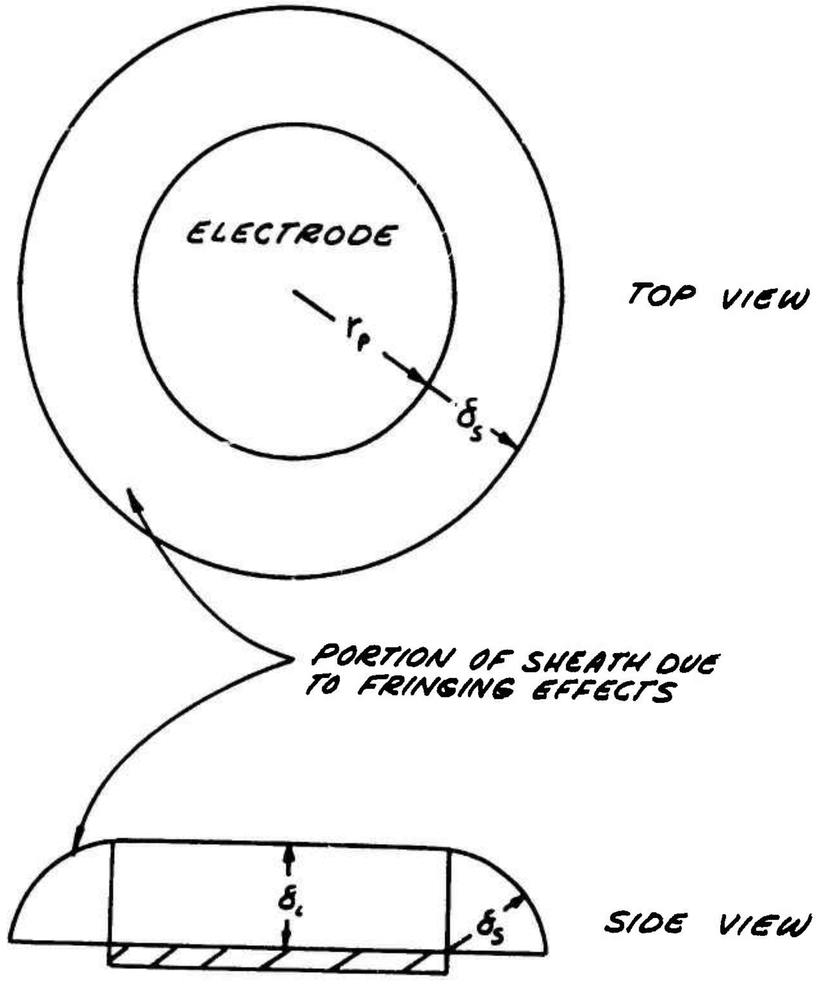

FIG. 21 CALCULATED SHEATH THICKNESS δ_s vs DISTANCE SL ALONG BODY IF $J_c = J_{exp}$

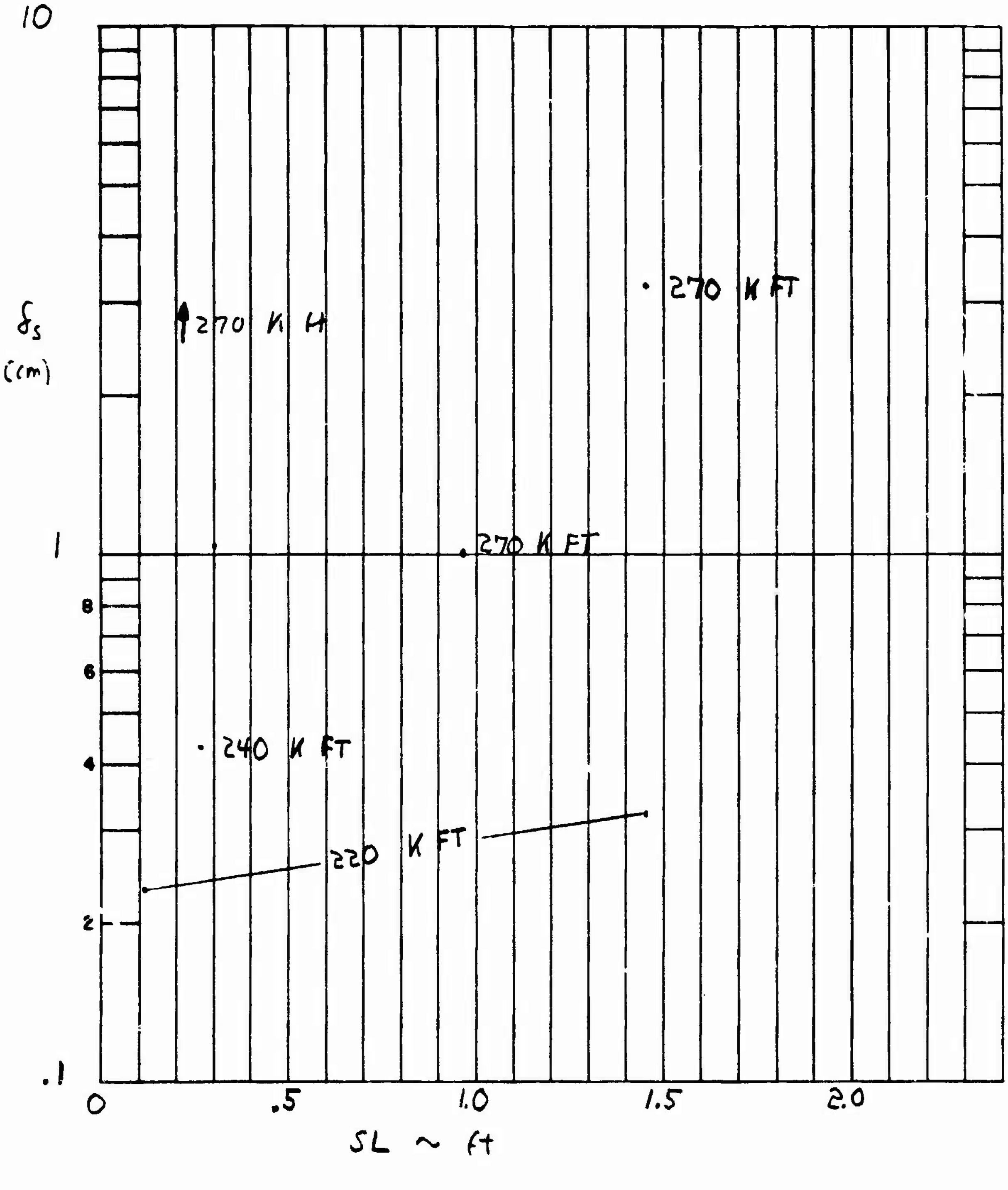

FIG. 22 COMPARISON BETWEEN DIFFUSION CURRENT j_{diff} AND THERMAL DRIFT CURRENT j_{th} AT

$z = 270$ K ft $s = .37$ ft

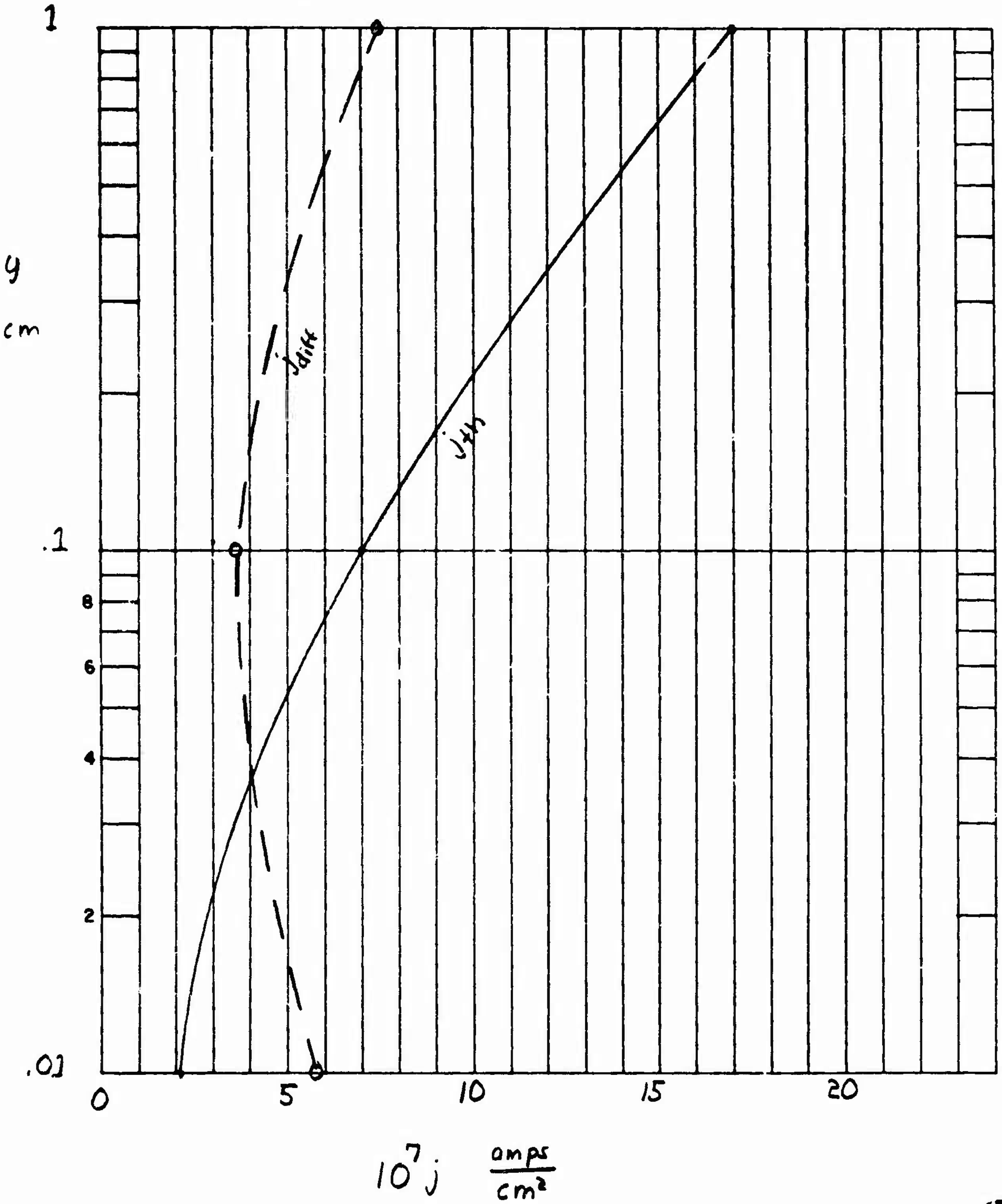

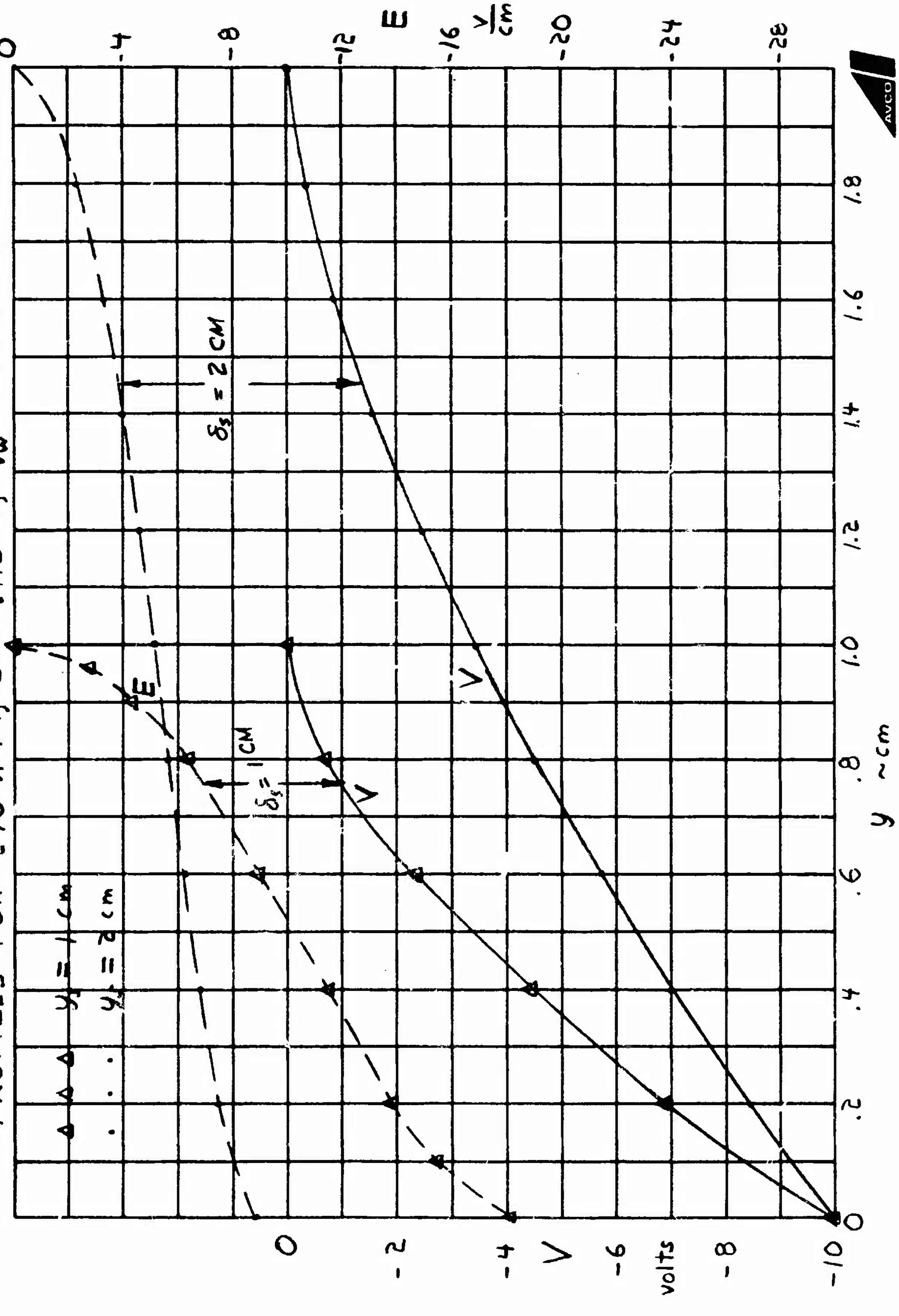

FIG 23 POTENTIAL FIELD V AND ELECTRIC FIELD E PROFILES FOR 270 K FT, S = .113 m, V_w = −10 volts